NASA Contractor Report 4446

Towards Understanding Turbulent Scalar Mixing

Sharath S. Girimaji

CONTRACT NAS1-18599
JULY 1992

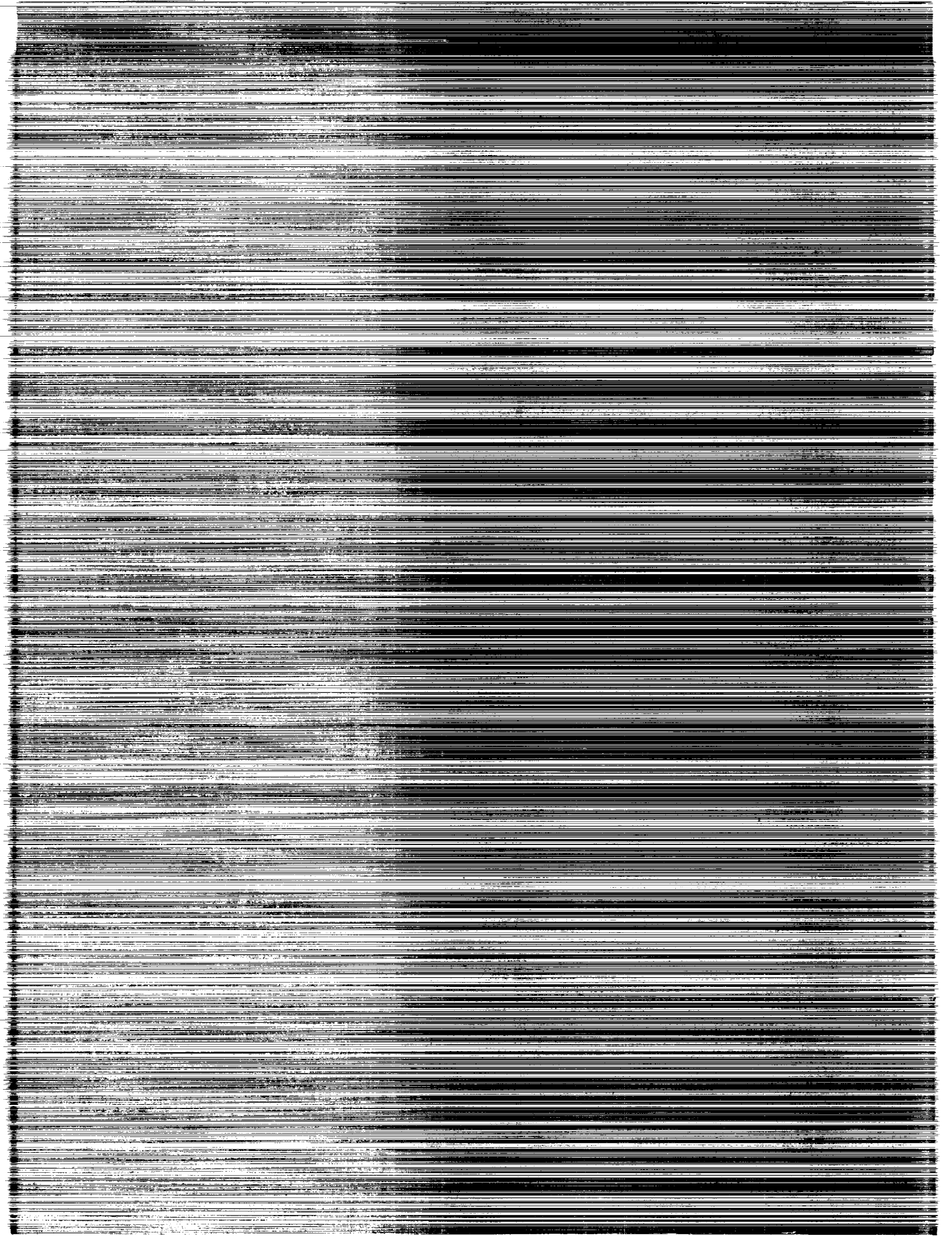

NASA Contractor Report 4446

Towards Understanding Turbulent Scalar Mixing

Sharath S. Girimaji
Analytical Services & Materials, Inc.
Hampton, Virginia

Prepared for
Langley Research Center
under Contract NAS1-18599

National Aeronautics and
Space Administration
Office of Management
Scientific and Technical
Information Program
1992

Towards understanding turbulent scalar mixing

Sharath S. Girimaji
A. S. & M. Inc., Hampton, Virginia 23666

Abstract

In an effort towards understanding turbulent scalar mixing, we study the effect of molecular mixing, first in isolation and then accounting for the effects of the velocity field. The chief motivation for this approach stems from the strong resemblance of the scalar probability density function (pdf) obtained from the scalar field evolving from the heat conduction equation and that evolving in a turbulent velocity field. However, the evolution of the scalar dissipation is different for the two cases. We attempt to account for these differences, which are due to the velocity field, using a Lagrangian frame analysis. After establishing the usefulness of this approach, we use the heat-conduction simulations (HCS), in lieu of the more expensive direct numerical simulations (DNS), to study many of the less understood aspects of turbulent mixing. Comparison between the HCS data and available models are made whenever possible. It is established that the β pdf characterizes, quite well, the evolution of the scalar pdf during mixing from all types of non-premixed initial conditions.

1 Introduction

Diffusion of smoke from chimneys into the atmosphere and mixing of fuel and air in an aircraft engine are but two of numerous instances in which scalars are convected and diffused in a turbulent flow field. Environmentalists and engineers alike are interested in understanding this mixing process. For many applications, a knowledge of the basic statistics of mixing suffices. However, when scalar mixing is accompanied by chemical reaction, a detailed understanding of the probability density function (pdf) of the scalars is required (Pope 1985). The direct numerical simulations (DNS) of Eswaran and Pope (1988) (referred to as EP henceforth) gave us the first close look at the details of the evolution of the scalar pdf in constant density isotropic turbulence. Since then, there have been other DNS studies of passive scalar mixing and mixing with chemical reactions (Givi 1989). These DNS data, apart from enhancing our understanding of turbulent mixing, also provide a test bed for evaluating mixing models. The mapping closure model (Chen, Chen and Kraichnan 1989, Pope 1991, Gao 1991) has been strongly validated by DNS data and has emerged as the leading turbulent-mixing model. The β-pdf model for scalar mixing (Girimaji 1991a, 1992) represents an instance of the direct use of DNS observations to formulate simplified closure models for problems of practical importance such as turbulent combustion (Girimaji 1991b). Despite these recent long strides, our understanding of turbulent mixing remains incomplete.

A popular technique often used in the past to understand turbulent processes is the study of the process in related simpler systems (e.g., use of Burger's equation rather than Navier-Stokes). In the same vein, we first

study the evolution of initially-random scalar fields evolving according to the heat conduction equation rather than the full scalar evolution equation. Then we account for the effect of the velocity field using a Lagrangian frame analysis where these effects are related to the material-element deformation characteristics of the turbulent velocity field.

1.1 Motivation

We study the evolution of a scalar field $\phi(\mathbf{x}, t)$ subject to the heat conduction equation,

$$\frac{\partial \phi}{\partial t} = D \frac{\partial^2 \phi}{\partial x_i \partial x_i}, \tag{1}$$

rather than the full evolution equation,

$$\frac{\partial \phi}{\partial t} + u_i \frac{\partial \phi}{\partial x_i} = D \frac{\partial^2 \phi}{\partial x_i \partial x_i}, \tag{2}$$

where D is the coefficient of Fickian diffusion and $\mathbf{u}(\mathbf{x}, t)$ is the velocity field. There are several *a priori* motivations to perform such a study to better our understanding of turbulent mixing. For example, irrespective of whether the scalar field evolves according to equation (1) or (2), the scalar-pdf ($F(\phi)$) evolution equation is the same. In either case, the pdf evolves in an isotropic turbulent field according to (Pope 1985)

$$\frac{\partial F(\psi)}{\partial t} = -\frac{\partial^2}{\partial \psi \partial \psi}\{F(\psi)\chi(\psi)\}, \tag{3}$$

where ψ is the probability-space value of the scalar concentration and the conditional scalar dissipation $\chi(\psi)$ is given by

$$\chi(\psi) = D\langle \frac{\partial^2 \phi}{\partial x_i \partial x_i} | \phi = \psi \rangle. \tag{4}$$

The notation $\langle b|r\rangle$ is used to denote the conditional expectation of b with respect to r. For the purpose of analyzing the evolution of the scalar pdf, it is clear from equation (3) that time t can be simply rescaled to account for the diffusion coefficient and the diffusivity can be assumed to be unity without loss of generality.

A strong *a posteriori* motivation for this study comes from our observation that the pdf's calculated from equation (1) (for the case of equal-quantity, non-premixed initial condition) at various stages of scalar decay are quite similar to those obtained from the DNS study of EP at the corresponding values of scalar variance. It should be recalled here that one of the principal findings of the DNS study is that the shapes adopted by the scalar pdf are independent of the initial scalar length scale. That is, at any stage of scalar decay characterized by the value of variance, the shape of the scalar pdf is independent of the initial scalar length scale and turbulence statistics. At any given value of scalar variance, we find that the scalar pdf obtained from the heat conduction equation is quite similar to the scale-independent pdf in the turbulent field obtained by EP.

Role of the velocity field. As a prelude to our study, we first attempt to understand the role of the velocity field in turbulent scalar mixing. The role of the velocity field can be most easily understood from the spectral version of equation (2),

$$\frac{\partial\tilde{\phi}(\mathbf{k},t)}{\partial t} = -\sqrt{-1}\int_{-\infty}^{\infty} m_i\tilde{u}_i(\mathbf{k}-\mathbf{m},t)\tilde{\phi}(\mathbf{m},t)d\mathbf{m} - k^2\tilde{\phi}(\mathbf{k},t), \qquad (5)$$

where a tilde denotes the Fourier transform of the quantity and $\mathbf{k}$ is the wavenumber vector of magnitude k. From this equation we can glean that,

when the length scale of the velocity field (l_u) is much larger than that of the scalar field (l_s), the effect of the velocity field is negligible. On the other hand, when the length scales are comparable, or when the scalar length scale is larger, the velocity field cascades the scalar energy down to smaller scales until molecular diffusion ultimately takes over. However, this rearrangement of scalar spectrum is such that the scalar statistics in the physical space are unaffected. So, it is clear that in the former case when $l_u/l_s \gg 1$, the neglect of the velocity field is quite reasonable, whereas in the latter case ($l_u/l_s \leq 1$), the consequences of its omission are unclear. EP find that over a wide range of the initial scalar length scales ($l_u/l_s \sim 1$ to 16) the evolution of the shape of the pdf is similar although the time scales of evolution are vastly different. This clearly implies that the velocity field has little influence on the scalar pdf shapes. Therefore, our present study of turbulent mixing using the heat-conduction equation (which represents $l_u/l_s \to \infty$) should be meaningful at least in understanding the evolution of the shape of the scalar pdf.

In the presence of a velocity field, the scalar gradient evolves according to

$$\frac{\partial}{\partial t}\frac{\partial \phi}{\partial x_j} + u_i \frac{\partial}{\partial x_i}\frac{\partial \phi}{\partial x_j} = -\frac{\partial u_i}{\partial x_j}\frac{\partial \phi}{\partial x_i} + \frac{\partial^2}{\partial x_i \partial x_i}\frac{\partial \phi}{\partial x_j}. \tag{6}$$

The effect of the velocity field on the scalar gradient is not only to rearrange its spectral content, but also to affect its physical-space pdf, owing to the presence of the first term on the right-hand side (RHS). The evolution of the scalar-gradient pdf, F(**g**), where **g** is the probability-space counterpart of the scalar gradient vector, is given by

$$\frac{\partial F(\mathbf{g})}{\partial t} = -\frac{\partial}{\partial g_i}[F(\mathbf{g})\langle -\frac{\partial u_i}{\partial x_j}\frac{\partial \phi}{\partial x_i} + \frac{\partial^2}{\partial x_i \partial x_i}\frac{\partial \phi}{\partial x_j}|\mathbf{g}\rangle]. \tag{7}$$

So, it is clear that the velocity gradients directly affect the evolution of the scalar-gradient pdf and, hence, that of the scalar dissipation, θ $(= \frac{\partial \phi}{\partial x_i}\frac{\partial \phi}{\partial x_i})$. However, the effect of the velocity field on the scalar pdf is only indirect, via the scalar gradients.

The scalar variance σ^2 evolves according to

$$\frac{d\sigma^2}{dt} = -\langle \frac{\partial \phi}{\partial x_i}\frac{\partial \phi}{\partial x_i} \rangle \equiv -\epsilon_s, \tag{8}$$

where ϵ_s is the mean scalar dissipation. So, the velocity field affects the evolution of the variance via its effect on ϵ_s.

1.2 Numerical Aspects

The solution for equation (1) has long been known in integral form for general initial conditions and in closed form for many simple initial conditions. The object of this study is to perform detailed statistical analysis of the behavior of the solution of equation (1) evolving from random initial conditions. As mentioned before, we expect such a study to shed light on many aspects of turbulent mixing.

In this paper, we restrict our attention to constant-density, isotropic, two-scalar mixing. Without loss of generality, we can assume the concentration of one of the scalars to be $\phi(\mathbf{x}, t)$ $(0 \leq \phi \leq 1)$ and that of the other to be $(1 - \phi)$. Since only one of the concentrations is an independent variable, it suffices to study the statistics of either one of the fields. In constant-density turbulence, scalar concentration and scalar mass fraction are equivalent and, hence, throughout this paper we use the terms synonymously.

The computational domain is a cubical box with periodic boundary conditions. The initial scalar field is random in nature. Owing to the complexity of the initial conditions, only a numerical solution to the heat equation is possible. The Fourier coefficient of each wavenumber evolves independently, and its value at any time t is given by

$$\tilde{\phi}(\mathbf{k},t) = \tilde{\phi}(\mathbf{k},0)e^{-k^2 t}. \tag{9}$$

Hence, even time stepping is not necessary. Knowing the initial field, the Fourier coefficients at any required time t are determined using the above equation. Then, the scalar information is transformed to physical space and all the required statistics are evaluated.

The initial conditions are specified in a manner similar to that of EP. The procedure involves three steps.

1. First, the Fourier coefficients of various wavenumbers are assigned values according to

$$\tilde{\phi}^*(\mathbf{k}) = f(\mathbf{k})exp[2\pi i\alpha(\mathbf{k})], \tag{10}$$

where $\alpha(\mathbf{k})$ is a random variable distributed uniformly between zero and unity. The function $f(\mathbf{k})$ is given by

$$f(\mathbf{k}) = \begin{cases} 1 \text{ for } k_s - 3 \leq k \leq k_s + 3 \\ 0 \text{ otherwise.} \end{cases} \tag{11}$$

The central wavenumber, k_s, of the scalar energy containing range is determined from the prescribed initial scalar length scale according

to

$$k_s = \frac{2\pi}{l_s}. \tag{12}$$

2. The scalar field in transformed into the physical space, yielding $\phi^*(\mathbf{x})$.

3. The initial scalar field $\phi(\mathbf{x}, t)$ is now assigned from the field $\phi^*(\mathbf{x})$, depending upon the initial pdf required. For example, if we need the initial pdf to be

$$F(\psi, 0) = \frac{1}{2}[\delta(\psi) + \delta(1 - \psi)], \tag{13}$$

then the scalar values are assigned according to

$$\phi(\mathbf{x}, 0) = \begin{array}{l} 1 \text{ if } \phi^*(\mathbf{x}) \geq 0, \\ \\ 0 \text{ if } \phi^*(\mathbf{x}) < 0. \end{array} \tag{14}$$

A triple-delta initial condition can be obtained as follows:

$$\phi(\mathbf{x}, 0) = \begin{array}{l} 1 \text{ if } \phi^*(\mathbf{x}) \geq q, \\ 0.7 \text{ if } q > \phi^*(\mathbf{x}) \geq r, \\ 0 \text{ otherwise,} \end{array} \tag{15}$$

which produces the initial pdf

$$F(\psi) = a_1\delta(\psi) + a_2\delta(\psi - 0.7) + (1 - a_1 - a_2)\delta(\psi - 1), \tag{16}$$

where a_1 and a_2 depend upon the values of q and r. Thus, we can obtain an isotropic, random initial scalar field of prescribed length scale and pdf.

The number of scalar energy containing wavenumber nodes is different for different values of k_s: the larger the initial scalar length scale, the smaller is the number of energy containing wavenumber nodes. Since there is no cascading mechanism in the heat conduction equation, the number of energy containing nodes is the same at all times for any given initial length scale.

All the results presented in this paper are from simulations using either 64^3 or 128^3 grid points. For the calculation of the scalar moments, it is found that 64^3 simulations are adequate. For the calculations of the pdf's and scalar dissipation statistics, 128^3 simulations are used. For the sake of accuracy, scalar gradients are first formed in Fourier space, then transformed to physical space, and finally used to calculate the scalar dissipation statistics. The scalar pdf's were calculated from 200 equal-sized bins in the range (0, 1).

Outline. First, we establish the similarities and the differences between molecular mixing with and without the turbulent velocity field. We achieve this by comparing the heat-equation data with the DNS data for the case of equal-quantity, non-premixed, two-scalar mixing. Then, we use these findings to effect simplifications in a Lagrangian frame analysis of turbulent scalar mixing – in an effort to account for the role of the velocity field. After establishing the usefulness of this approach, we use the heat-conduction equation to study the statistical behavior of scalar fields evolving from a variety of other important initial conditions. The data from these heat-conduction simulations (HCS) are then used to evaluate aspects of turbulent mixing models which have hitherto been untested, owing to the lack of corresponding DNS data. Another objective of the paper is to determine if the

β pdf, which was found to characterize the equal-quantity, non-premixed, scalar pdf quite well (Girimaji 1991a), can adequately replicate the scalar pdf for non-equal-quantity mixing also.

The remainder of the paper is organized as follows. In Section 2, we study the equal-quantity, non-premixed mixing. In Section 3, we perform the Lagrangian frame analysis to account for the effects of the velocity field. In Section 4, we study non-equal ($\mu \neq 0.5$), non-premixed initial fields and partially-mixed initial fields. We conclude with a summary in Section 5.

2 Equal-quantity, non-premixed mixing

In this Section, we present the results of equal-quantity, non-premixed scalar fields evolving by the heat conduction equation. As the pdf evolves from the double-delta initial condition, the mean scalar mass-fraction (μ) remains constant at 0.5. Comparisons with the DNS of Eswaran and Pope (1988), the β-pdf model of Girimaji (1991a), the scalar-dissipation model of O'Brien and Jiang (1991), and the scalar-dissipation model of Girimaji (1992) are made wherever appropriate.

2.1 Evolution of scalar statistics

In Figure 1, the pdf of scalar mass fraction obtained from the heat conduction simulation (HCS, $k_s = 8$), the DNS ($k_s = 8$) of Eswaran and Pope (1988), and the β-pdf model of Girimaji (1991a) are compared at various stages of mixing. While comparing the results, it is important to recognize that the initial spectral fields of the HCS and DNS are slightly different. The high wavenumber components of the DNS initial field are modified to

yield somewhat smooth initial fields. The HCS initial field is unsmoothed. So, the DNS data at each level of scalar mixing may represent the pdf at a slightly more advanced stage of decay than the corresponding HCS or the model pdf. The jaggedness in the early-time HCS pdf is due to the presence of the untruncated high wavenumber components of the scalar field. Given all these factors, the agreement is quite good. Both HCS and the model capture the various phases of the DNS evolution well.

The main inference from the DNS study is that, irrespective of the initial scalar length scale (l_s), the shape of the scalar pdf at any given stage of decay is the same. This means that in turbulent mixing the normalized scalar moments are unique functions of the scalar variance, independent of l_s. This brings up the question, are the normalized scalar-moments obtained from HCS also unique functions of scalar variance? In Figure 2a, the HCS flatness-factor is plotted as a function of variance (σ^2), for various k_s ranging from 1 to 16. Except for the cases of $k_s = 1$ and $k_s = 2$, the plots do collapse to within statistical error. The flatness-factor of $k_s = 1$ and $k_s = 2$ do collapse at the early stages of mixing but at later times show a small but distinct deviation to lesser values. This is in disagreement with the DNS results which indicate that the pdf shapes are the same for the entire range of k_s (1 through 16). The difference can be attributed to the effect of the velocity field. As was seen in the previous Section, the scalar-energy cascade (due to velocity gradients) is particularly important for small k_s. In real turbulence, the scalar spectrum for these cases would shift to larger wavenumbers, and the evolution subsequently would be the same as that of larger k_s. As for larger k_s, the flatness-factor asymptotes to a Gaussian value of 3 during the latter stages of mixing. It remains nearly 3 for about three

decades of variance and then falls off to smaller values for $\sigma^2 > 10^{-5}$ (not shown). This behavior was also observed by Gao (private communication) in the DNS of turbulent scalar mixing. Furthermore, at very small variance values, the statistical and numerical errors involved become too large to compute the high-order moments accurately. In any event, this completely-mixed limit is of lesser practical value and, hence, has not been investigated further. In Figure 2b, the super-skewness of the same cases as in Figure 2a are compared. Again for $k_s > 2$, we have collapse. During the latter stages of mixing ($10^{-5} \leq \sigma^2 \leq 10^{-3}$), the super-skewness is close to the Gaussian value of 15.

The main inferences from Figures 1 and 2 are

1. The HCS captures the details of the DNS scalar pdf evolution for $k_s = 8$ (Figure 1).

2. For large enough k_s (> 2), the HCS-pdf evolution is *universal* (i.e., same for all k_s; see Figure 2). The universal evolutions of HCS and DNS must be the same, considering the good agreement between HCS and DNS for the case of $k_s = 8$. Hence, the velocity field does not affect the shape of the scalar pdf for large enough k_s (small l_s).

3. For $k_s < 2$, the velocity field affects the shape of the scalar pdf but modifies it only slightly. For most practical purposes, this modification can perhaps be neglected.

4. The β-pdf model captures the *universal* evolution remarkably well.

Evolution of ϕ_{min} and ϕ_{max}. The quantities ϕ_{min} and ϕ_{max} are the global minimum and maximum values of the scalar concentration at any given time. The evolution of these are of particular interest in the context of the evolution of conditional scalar dissipation. It is shown in Girimaji (1992) that the values of conditional dissipation at ϕ_{min} and ϕ_{max} are zero. The pdf value is zero outside the range (ϕ_{min}, ϕ_{max}). The conditional scalar dissipation model of O'Brien and Jiang (1991) implies that ϕ_{min} and ϕ_{max} do not change in time.

For the problem under consideration (periodic scalar field with initial double-delta pdf), the exact solution is

$$\phi(\mathbf{x},t) = \frac{1}{2} + \frac{1}{\sqrt{2\pi}} \sum_{|k|=1}^{\pm\infty} \tilde{\phi}(\mathbf{k},0) exp[-k^2 t] exp[\sqrt{-1}\mathbf{k}.\mathbf{x}] d\mathbf{k}, \qquad (17)$$

where $\tilde{\phi}(\mathbf{k},0)$ is determined from the initial conditions. At time $t = 0$, the ϕ_{min} and ϕ_{max} are clearly zero and unity. With time, the value of ϕ at all $\mathbf{x}$ locations changes. The fastest change comes about at a location which has the highest small-scale contribution. The slowest change is at a location where the large-scale contribution is the highest. From this we can surmise the following:

$$\phi_{max}(t) \leq \frac{1}{2} + \frac{1}{2} exp[-t], \qquad (18)$$

$$\phi_{min}(t) \geq \frac{1}{2} - \frac{1}{2} exp[-t]. \qquad (19)$$

In Figure 3, the temporal evolution of ϕ_{min} and ϕ_{max} for various k_s are plotted. The rate of decay of ϕ_{max} increases with k_s. Similarly, the growth rate of ϕ_{min} increases with k_s. The above inequalities (equations 18 and 19) are satisfied for all k_s. At early times, the data shows some violation of

the inequalities. This is an artifact of truncating the infinite Fourier series (Gibb's phenomena) and is unphysical. At latter times when the influence of the high wavenumbers dies out, the inequalities are satisfied by the scalar field. In any event it is clear that the range of the scalar concentration over which the pdf is non-zero decreases with time.

In the presence of a turbulent field, the amplitude of various wavenumbers decay in an unknown fashion. However, we still have the following inequalities,

$$\phi_{max}(t) - \frac{1}{2} \leq \frac{1}{\sqrt{2\pi}} \sum_{|k|=1}^{\pm\infty} |\tilde{\phi}(\mathbf{k}, t)| \tag{20}$$

$$\frac{1}{2} - \phi_{min}(t) \leq \frac{1}{\sqrt{2\pi}} \sum_{|k|=1}^{\pm\infty} |\tilde{\phi}(\mathbf{k}, t)|. \tag{21}$$

The variance at time t is given by

$$\sigma^2(t) = \frac{1}{2\pi} \sum_{|k|=1}^{\pm\infty} [\tilde{\phi}(\mathbf{k}, t)]^2. \tag{22}$$

Initially, ϕ_{max} and ϕ_{min} are unity and zero, and the variance is some finite quantity. With mixing, the variance decreases, going to nearly zero at infinite time:

$$\sigma^2(t \to \infty) = \frac{1}{2\pi} \sum_{|k|=1}^{\pm\infty} [\tilde{\phi}(\mathbf{k}, t = \infty)]^2 \to 0, \tag{23}$$

so that,

$$\sum_{|k|=1}^{\pm\infty} |\tilde{\phi}(\mathbf{k}, t = \infty)| \to 0. \tag{24}$$

As a result we have

$$\phi_{max}(t = \infty) \to \frac{1}{2}, \tag{25}$$

$$\phi_{min}(t = \infty) \to \frac{1}{2}. \tag{26}$$

Hence, even in the presence of a turbulent velocity field we can expect the non-zero range of the pdf to decrease, contrary to the implications of the mapping closure solution of O'Brien and Jiang (1991).

2.2 Conditional scalar dissipation

As was seen in the Introduction, the evolution of the scalar pdf is determined by the conditional scalar dissipation, $\chi(\psi)$ (equation 3). The mean scalar dissipation, ϵ_s, in terms of the conditional scalar dissipation, is

$$\epsilon_s \equiv \langle \frac{\partial \phi}{\partial x_i} \frac{\partial \phi}{\partial x_i} \rangle = \int_0^1 \chi(\psi) F(\psi) d\psi. \tag{27}$$

While the conditional dissipation ratio, $\chi(\psi)/\epsilon_s$, plays an important role in the evolution of the shape of the scalar pdf, the rate of the evolution is determined by ϵ_s.

Models. The models against which the HCS and DNS data are compared are: model M1, the β-pdf conditional dissipation ratio model of Girimaji (1992), and model M2, the model for normalized conditional dissipation, $\chi(\psi)/\chi(0.5)$ (O'Brien and Jiang 1991). The model M1 is given by,

$$\frac{\chi(\psi)}{\epsilon_s} = -2 \frac{\mu(1-\mu)}{\sigma^4} \frac{I(\psi)}{F(\psi)}, \tag{28}$$

where $I(\psi)$ is given by

$$I(\psi) = \int_0^\psi [\mu\{\ln \psi' - \langle \ln \phi \rangle\} + (1-\mu)\{\ln(1-\psi') - \langle \ln(1-\phi) \rangle\}] F(\psi')(\psi - \psi') d\psi'. \tag{29}$$

The model M2 is given by

$$\frac{\chi(\psi)}{\chi(0.5)} = exp[-2\{erf^{-1}(2\psi - 1)\}^2], \tag{30}$$

where erf^{-1} represents the inverse error function. The most striking feature of the model M2 is that it is independent of the current scalar pdf.

In Figure 4, the conditional dissipation ratios of HCS, DNS, and the conditional dissipation model of Girimaji (1992) are plotted against normalized mass fraction. The calculation of any high-order conditional statistic - like χ/ϵ_s - from numerical data is usually fraught with statistical errors. Taking this into consideration, the agreement between HCS and DNS is good for the early stage ($\sigma = 0.27$) and adequate for the intermediate stage ($\sigma = 0.1$) of mixing. At the final stages of mixing, the conditional dissipation ratio of the HCS data is nearly constant over the range of mass fraction considered. This is consistent with the fact that the HCS scalar pdf decays as a Gaussian at this range of variance. The DNS conditional dissipation ratio is minimum at $\psi = 0.5$ and increases steeply for other values; this trend is inconsistent with the observed Gaussianity of the scalar pdf and is probably due to statistical error. The HCS data comes from a 128^3 simulation and, hence, can be expected to be statistically more accurate than the DNS data which comes from a 64^3 simulation. The model M1 agrees well with both HCS and DNS data during early and intermediate stages of mixing and shows the same trend as the HCS data at the latter stages.

The above comparison between the model, HCS, and DNS data is only over a narrow range of mass fraction. In Figure 5, the normalized conditional dissipation $\chi(\psi)/\chi(0.5)$ of HCS is compared with the models M1 and M2 over the entire range of mass fraction. The models agree with HCS data during the early stages of mixing ($\sigma^2 > 0.05$). During the latter stages (when $\phi_{max} < 1$ and $\phi_{min} > 0$), the agreement is not as good. The HCS values are set to zero outside the range (ϕ_{min}, ϕ_{max}). In the middle of the

range, the agreement is adequate, whereas near the edges, it is poor. This disagreement near the edges of the range (ϕ_{min}, ϕ_{max}) could be due to statistical error in HCS data. Near the edges the probability of ψ is so low that at these values of mass fraction there are very few samples of scalar dissipation from which to compute the conditional dissipation. This statistical error makes it difficult to completely comprehend the evolution of conditional dissipation at the edges. However, it can be surmised from the earlier findings about $\phi_{min}(t)$ and $\phi_{max}(t)$ that the zero values of the conditional dissipation migrate inwards (from 0 and 1) with increased mixing.

To circumvent the problem of too few statistical samples at the edges of the scalar range, in Figure 6, we plot the fractional scalar dissipation, $\frac{F(\psi)\chi(\psi)}{\epsilon_s}$, of the HCS data and model M1. The advantage of plotting this quantity is that when the statistical error is high due the low probability, the conditional dissipation is weighted down by the probability density itself. Here, the agreement between the HCS data and the β-pdf-based model M1 is excellent. The jagged nature of the HCS-data plot at the earliest time is again due to the presence of very high wavenumber components in the scalar field. With time, the high wavenumber components die out quickly, yielding smooth statistics.

Apart from the mathematical convenience it offers, the fractional scalar dissipation is a physically important quantity. It is this quantity, rather than the conditional dissipation alone, that determines the evolution of the scalar pdf (equation 3). In fact, the conditional dissipation always appears along with the probability density function (equation 27). This suggests that our efforts should be directed towards modeling fractional

scalar dissipation rather than conditional scalar dissipation. Moreover, the value of conditional dissipation outside the range (ϕ_{min}, ϕ_{max}) is irrelevant.

Our inferences from Figures 4 - 6 are

1. The conditional dissipation ratio, $\chi(\psi)/\epsilon_s$, calculated from the DNS, the HCS, and the model M1 agree adequately well.

2. The normalized conditional dissipation, $\chi(\psi)/\chi(0.5)$, of the models M1 and M2 agree well with HCS data during the early stages of mixing. At long times, the statistical error at the edges of the scalar range are too large to make a valid comparison. For this same reason, it is difficult to evaluate whether the normalized conditional dissipation always has a constant form (as suggested by the mapping-closure-based conditional-dissipation model of O'Brien and Jiang 1991), or if it tends to thin down with time, asymptoting to a spike shape at $\psi = 0.5$ (as suggested by Girimaji 1992). However, since ϕ_{min} and ϕ_{max} both tend towards the mean at long times (Figure 3), it appears that the latter is the more probable scenario.

3. The fractional dissipation ratio, $\frac{F(\psi)\chi(\psi)}{\epsilon_s}$, of the HCS and the model M1 show excellent agreement. Since it is this quantity that determines the scalar evolution, the agreement is of significance.

2.3 Evolution of scalar variance and mean scalar dissipation

The evolution of scalar variance (σ^2) and the mean scalar dissipation (ϵ_s) obtained from HCS for various initial length scales are plotted in Figure 7. To precisely understand the effect of the velocity field on the evolution

of these quantities, we compare Figure 7 with the corresponding DNS data of Eswaran and Pope (1988, Figures 11 and 12). The biggest difference between the HCS and DNS data is in the evolution of ϵ_s. For all k_s, the HCS-ϵ_s decreases monotonically in time, as expected. However, the DNS-ϵ_s shows a non-monotonic evolution for small k_s. For $k_s \leq 4$, the DNS mean scalar dissipation increases in the beginning. After peaking, the mean scalar dissipation decays, gradually at first and then more rapidly. This non-monotonic behavior is more pronounced for smaller k_s. The implication of this on the variance evolution is that the DNS decay rate is higher than that of HCS for small k_s.

The above phenomenon, which is entirely due to the velocity field, is discussed in the next Section, where the effects of the velocity field are accounted for.

2.4 Pdf of scalar gradient

If the scalar evolves according to the heat-conduction equation, the scalar gradient also evolves according to the heat-conduction equation. However, the initial conditions of these fields are quite different. Due to discontinuities in the initial scalar field, the initial scalar-gradient field is composed of delta functions. In Figure 8, the evolution of the flatness-factor and superskewness of scalar-gradient component $\partial\phi/\partial x_1$ is shown for $k_s = 8$ and $k_s = 16$. For both cases, the moments approach Gaussian values at long times. The scalar-dissipation pdf (not shown) is, however, far from Gaussian. Eswaran and Pope (1988) find that the scalar dissipation is log-normally distributed. This log-normality is a consequence of the velocity field and is discussed in detail in the next Section.

3 Accounting for the effects of velocity field

In this Section, we attempt to account for the effect of the turbulent velocity field on scalar mixing. Findings from the previous Section are invoked to effect simplifying assumptions in our analysis.

The effect of the velocity field is most easily accounted for in the Lagrangian frame of reference (**x**, t). Consider the evolution of the scalar field in a turbulent velocity field **U**(**X**, t). In this Section, we designate the Eulerian coordinates as **X**, rather than **x**, as was done in the previous Sections. Let the coordinate system evolve according to

$$\frac{\partial \mathbf{X}(\mathbf{x},t)}{\partial t} = \mathbf{U}[\mathbf{X}(\mathbf{x},t),t], \tag{31}$$

with the initial condition,

$$\mathbf{x} = \mathbf{X}(0). \tag{32}$$

The velocity field **U**(**X**,t) evolves according to the Navier-Stokes equation. Now, let the Lagrangian coordinate system **x** be Cartesian. Then, the Eulerian system **X** is nonstationary, curvilinear, and nonorthogonal. In the coordinate system following fluid particles, the scalar concentration evolves according to

$$\frac{\partial \phi(\mathbf{x},t)}{\partial t} = D\frac{\partial^2 \phi(\mathbf{X},t)}{\partial X_i \partial X_i}, \tag{33}$$

where D is scalar diffusivity. The molecular diffusion can be rewritten in terms of the Lagrangian scalar derivatives:

$$\frac{\partial \phi(\mathbf{x},t)}{\partial t} = D\frac{\partial x_a}{\partial X_i}\frac{\partial x_b}{\partial X_i}\frac{\partial^2 \phi(\mathbf{x},t)}{\partial x_a \partial x_b}. \tag{34}$$

The evolution equation of the pdf, $G(\psi_l, t)$, of the scalar concentration $\phi(\mathbf{x}, t)$ following fluid particles in an isotropic field can be derived using standard methods (Pope 1985):

$$\frac{\partial G(\psi_l,t)}{\partial t} = -D\frac{\partial^2}{\partial\psi_l\partial\psi_l}[G(\psi_l,t)\langle\frac{\partial x_a}{\partial X_i}\frac{\partial x_b}{\partial X_i}\frac{\partial\phi(\mathbf{x},t)}{\partial x_a}\frac{\partial\phi(\mathbf{x},t)}{\partial x_b}|\phi=\psi_l\rangle]. \quad (35)$$

(In the absence of the velocity field, the above equation reduces to equation (3)). Due to the isotropy of the field, the Lagrangian scalar pdf $G_l(\psi_l, t)$ and the Eulerian pdf $F(\psi, t)$ are identical.

Now we invoke the findings of the previous Section to simplify equation (35). It was found that, while the velocity field has a major effect on the time scale of scalar evolution, the pdf shapes during the evolution are unaltered for $k_s > 2$ and only slightly modified for $k_s \leq 2$. This, we argue, implies that the averaged effect of the velocity field conditioned upon the value of the scalar concentration is independent of the scalar value. That is, we suggest

$$\langle\frac{\partial x_a}{\partial X_i}\frac{\partial x_b}{\partial X_i}\frac{\partial\phi(\mathbf{x},t)}{\partial x_a}\frac{\partial\phi(\mathbf{x},t)}{\partial x_b}|\phi=\psi_l\rangle \approx \langle\frac{\partial x_a}{\partial X_i}\frac{\partial x_b}{\partial X_i}\rangle\langle\frac{\partial\phi(\mathbf{x},t)}{\partial x_a}\frac{\partial\phi(\mathbf{x},t)}{\partial x_b}|\phi=\psi_l\rangle, \quad (36)$$

where $\langle\frac{\partial x_a}{\partial X_i}\frac{\partial x_b}{\partial X_i}\rangle$ is independent of the scalar field. This is not such a far-fetched assumption, since the value of the scalar concentration is a strong function of the initial scalar field, which is independent of the velocity field.

Subject to the above assumption, equation (35) can be simplified as

$$\frac{\partial G(\psi_l,t)}{\partial t} \approx -D\langle\frac{\partial x_a}{\partial X_i}\frac{\partial x_b}{\partial X_i}\rangle\frac{\partial^2}{\partial\psi_l\partial\psi_l}[G(\psi_l,t)\langle\frac{\partial\phi(\mathbf{x},t)}{\partial x_a}\frac{\partial\phi(\mathbf{x},t)}{\partial x_b}|\phi=\psi_l\rangle]. \quad (37)$$

Owing to the isotropy of the turbulence field and the initial scalar field, we can further simplify as follows:

$$\langle \frac{\partial x_a}{\partial X_i} \frac{\partial x_b}{\partial X_i} \rangle = \frac{\delta_{ab}}{3} \langle \frac{\partial x_c}{\partial X_i} \frac{\partial x_c}{\partial X_i} \rangle \equiv \delta_{ab} \langle S \rangle. \tag{38}$$

Then,

$$\frac{\partial G(\psi_l, t)}{\partial t} \approx -\langle S \rangle \frac{\partial^2}{\partial \psi_l \partial \psi_l} [G(\psi_l, t) \chi_l(\psi_l)], \tag{39}$$

where $\chi_l(\psi_l)$ is the Lagrangian conditional scalar dissipation defined as

$$\chi_l(\psi_l) = D \langle \frac{\partial \phi(\mathbf{x}, t)}{\partial x_a} \frac{\partial \phi(\mathbf{x}, t)}{\partial x_a} | \phi = \psi_l \rangle. \tag{40}$$

Now we suggest that the effect of the velocity field on the evolution of $G(\psi_l, t)$ (and, hence, on $F(\psi, t)$) is only through the scalar $\langle S \rangle$, and that the Lagrangian conditional scalar dissipation is independent of the velocity field. Rescaling time as

$$\tau = \int_0^t \langle S(t) \rangle dt, \tag{41}$$

it is easily seen that the pdf evolution in the time coordinate τ is independent of the velocity field. The velocity-field-independent $\chi_l(\psi_l)$ is the conditional scalar dissipation of a scalar field evolving under the influence of the heat conduction equation (1) alone, from the same initial conditions as the full problem. Thus, the effects of molecular action and velocity field can be decoupled. Clearly, these simplifications will be accurate for $k_s > 2$, but less so otherwise.

Mean scalar dissipation, ϵ_s. In isotropic turbulence, the conditional dissipation of a scalar field can be approximated as (from equations 36 and 38)

$$\chi(\psi) = \langle \frac{\partial \phi}{\partial X_i} \frac{\partial \phi}{\partial X_i} | \phi = \psi \rangle = \langle S \rangle \chi_l(\psi_l). \tag{42}$$

The mean scalar dissipation is obtained by integrating equation (42):

$$\epsilon_s(t) = \langle S(t) \rangle \epsilon_l(t), \tag{43}$$

where

$$\epsilon_s(t) = D \langle \frac{\partial \phi}{\partial X_i} \frac{\partial \phi}{\partial X_i} \rangle,$$

and $\epsilon_l(t)$ is the mean scalar dissipation in an equivalent heat-conduction system:

$$\epsilon_l(t) = D \langle \frac{\partial \phi}{\partial x_a} \frac{\partial \phi}{\partial x_a} \rangle.$$

Some of the implications of this model are

1. **Case of zero diffusivity.** In this case, there is no evolution of the Lagrangian field. Hence, $\langle \frac{\partial \phi}{\partial x_a} \frac{\partial \phi}{\partial x_a} \rangle$ remains constant. However, due to the velocity field, $\langle S(t) \rangle$ will vary with time, and with it, $\langle \frac{\partial \phi}{\partial X_i} \frac{\partial \phi}{\partial X_i} \rangle$ will also change in time.

2. **Case of no velocity field.** For this case, $\langle S(t) \rangle$ is always unity and, hence, the problem reduces to the heat conduction equation, as it should.

3. $D \neq 0$ **and presence of velocity field.** In this case, the turbulent scalar dissipation changes in time due to the effect of the velocity field (*via* change in $\langle S(t) \rangle$) as well as due to the decay of the Lagrangian scalar field (*via* change in $\epsilon_l(t)$).

In order to understand the behavior of conditional scalar dissipation and mean scalar dissipation in turbulence, we need insight into the behavior of $\langle S(t) \rangle$ and $\epsilon_l(t)$. A study of the latter has already been performed in the previous Section. In the following subsection, we turn our attention to $\langle S(t) \rangle$.

3.1 Evolution of $\langle S(t) \rangle$

The scalar $S = \frac{1}{3}\frac{\partial x_a}{\partial X_i}\frac{\partial x_a}{\partial X_i}$, is a measure of the deformation of the coordinate frame caused by the velocity field. Differentiating equation (31) with respect to x_a, we get

$$\begin{aligned} \frac{\partial l_{ia}}{\partial t} &= \frac{\partial U_i(\mathbf{X}(\mathbf{x},t),t)}{\partial x_a} \\ &= \frac{\partial U_i}{\partial X_j} l_{ja}, \end{aligned} \tag{44}$$

where

$$l_{ia} = \frac{\partial X_i(\mathbf{x},t)}{\partial x_a}. \tag{45}$$

Equation (44) is the evolution equation of a material line element (Monin and Yaglom 1981). The quantity l_{ia} stands for the i-th component of the material line that was initially coincident with the x_a axis. Let $\mathbf{l}_a$ represent the line-element vector whose components are l_{1a}, l_{2a}, and l_{3a}. Recall that

$$\frac{\partial X_i(\mathbf{x},0)}{\partial x_a} = \delta_{ia}, \tag{46}$$

and, hence, $\mathbf{l}_a(\mathbf{x},0) = \mathbf{e}_a$, the unit vector along the x_a axis.

The material line element $\mathbf{l}_a$ is stretched (or shrunk) and reoriented by the velocity field. The line-element vector at any time t can be determined knowing the tensor $\mathbf{B}$ and the initial condition:

$$\mathbf{l}_a(t) = \mathbf{B}(t).\mathbf{e}_a. \tag{47}$$

The tensor $\mathbf{B}$ contains all of the one-point information of the fluid element and evolves according to (Monin and Yaglom 1981)

$$\frac{dB_{ij}}{dt} = \frac{\partial U_i}{\partial x_k} B_{kj}. \tag{48}$$

What is $S(t)$ in terms of l_{ia}? For evaluating S, we need the inverse of the matrix l_{ia}. Let L_{ia} be the inverse matrix; the components of this matrix in terms of l_{ia} are

$$\begin{aligned}
L_{11} &= \frac{1}{V}[l_{22}l_{33} - l_{23}l_{32}] = \frac{1}{V}(\mathbf{l}_2 \times \mathbf{l}_3).\mathbf{e}_1 = \frac{C_{11}}{V}, \\
L_{12} &= \frac{1}{V}[l_{32}l_{13} - l_{12}l_{33}] = \frac{1}{V}(\mathbf{l}_2 \times \mathbf{l}_3).\mathbf{e}_2 = \frac{C_{12}}{V}, \\
L_{13} &= \frac{1}{V}[l_{12}l_{23} - l_{22}l_{13}] = \frac{1}{V}(\mathbf{l}_2 \times \mathbf{l}_3).\mathbf{e}_3 = \frac{C_{13}}{V}, \\
L_{21} &= \frac{1}{V}[l_{23}l_{31} - l_{33}l_{21}] = \frac{1}{V}(\mathbf{l}_3 \times \mathbf{l}_1).\mathbf{e}_1 = \frac{C_{21}}{V}, \\
L_{22} &= \frac{1}{V}[l_{33}l_{11} - l_{31}l_{13}] = \frac{1}{V}(\mathbf{l}_3 \times \mathbf{l}_1).\mathbf{e}_2 = \frac{C_{22}}{V}, \\
L_{23} &= \frac{1}{V}[l_{21}l_{13} - l_{11}l_{23}] = \frac{1}{V}(\mathbf{l}_3 \times \mathbf{l}_1).\mathbf{e}_3 = \frac{C_{23}}{V}, \\
L_{31} &= \frac{1}{V}[l_{32}l_{21} - l_{31}l_{22}] = \frac{1}{V}(\mathbf{l}_1 \times \mathbf{l}_2).\mathbf{e}_1 = \frac{C_{31}}{V}, \\
L_{32} &= \frac{1}{V}[l_{31}l_{12} - l_{32}l_{11}] = \frac{1}{V}(\mathbf{l}_1 \times \mathbf{l}_2).\mathbf{e}_2 = \frac{C_{32}}{V}, \\
L_{33} &= \frac{1}{V}[l_{11}l_{22} - l_{12}l_{21}] = \frac{1}{V}(\mathbf{l}_1 \times \mathbf{l}_2).\mathbf{e}_3 = \frac{C_{33}}{V},
\end{aligned} \tag{49}$$

where V is the ratio of volume (or density) of the fluid element:

$$V(t) = \frac{\rho(t)}{\rho(0)} = exp[-\int_0^t \frac{\partial U_i}{\partial X_i}(t)dt]. \tag{50}$$

The numerator C_{ia} can be identified as the i-th component of area of a surface element whose normal is initially coincident with the x_a axis. The scalar S is then

$$S(t) = \frac{1}{3V}C_{ia}(t)C_{ia}(t) = \frac{1}{3V}[A_1^2(t) + A_2^2(t) + A_3^2(t)], \tag{51}$$

where A_a represents the magnitude of area of the material surface element whose normal is initially coincident with the x_a axis. For an incompressible velocity field, the density ratio V is always unity. The compressibility of

the velocity field manifests itself on the scalar mixing through V. The implication, then, is that the compressibility only affects the time scale of scalar evolution, without modifying the shape of the scalar pdf's. Indeed, Givi *et al* (1991) find that the β pdf replicates the scalar pdf in high-speed (compressible) mixing also.

For an isotropic velocity field, the various area magnitudes (A_1, A_2 and A_3) are all statistically equivalent. Hence, assuming isotropy,

$$\langle S(t) \rangle = \langle A^2(t) \rangle, \tag{52}$$

where $A(t)$ represents the area at any time t of any typical material-surface element (of initial unit area) associated with the fluid element.

A naive estimate of $\langle S(t) \rangle$ that ignores the effects of vorticity and strain-rate rotation can be made (*a la* Monin and Yaglom 1981). Subject to the above conditions (and incompressibility), we can expect

$$A(t) \sim exp[(a_1 + a_2)t], \tag{53}$$

so that

$$\langle S(t) \rangle \sim \exp[2(a_1 + a_2)t], \tag{54}$$

where a_1 and a_2 are the means of the positive and intermediate eigenvalues of the velocity gradient tensor. In real turbulence, however, the effects of vorticity and strain-rate rotation are important (Girimaji and Pope 1990).

Girimaji and Pope (1990) have performed extensive studies of the evolution of line, surface, and volume elements in statistically stationary, isotropic turbulence. One of their findings was that $\ln(A)$ has a Gaussian distribution, which implies that A^2 has a log-normal distribution. Although no

direct estimate of $\langle S(t) \rangle$ was made, based on the findings of that study, we can surmise some aspects of the behavior of $\langle S(t) \rangle$. Let us define

$$p(t) \equiv \frac{d \ln \langle S \rangle}{dt}, \tag{55}$$

so that we can write

$$\epsilon_s(t) \sim exp[\int_0^t p \, dt] \epsilon_l(t). \tag{56}$$

The exponential growth rate $p(t)$ is a function only of the turbulence parameters and is very likely to be positive at all times. In real turbulence, the temporal behavior of $p(t)$ is likely to be very similar to the line and area logarithmic growth rates (Girimaji and Pope 1990). At time $t = 0$, $p(t)$ will be nearly zero, owing to the lack of alignment between the material-element ellipsoid and the velocity-gradient tensor. As the alignment improves with time, $p(t)$ would increase, peaking at about $t_m = 5\tau_\eta$ (τ_η, Kolmogorov time scale), when the alignment between the principle axes of the velocity-gradient tensor and that of the material-element ellipsoid is at the maximum. Finally, as vorticity and the rotation of the strain-rate principal-axes reduce the alignment, p would asymptote to a lower value. Girimaji and Pope (1990) estimate the long-time growth rate of various moments of the area of surface elements and $p(t)$ has the form

$$p(t) = \frac{d \ln \langle A(t)^2 \rangle}{dt} \sim \frac{0.8}{\tau_\eta}. \tag{57}$$

Implications of the behavior of $\langle S(t) \rangle$ on $\epsilon_s(t)$. The Lagrangian dissipation $\epsilon_l(t)$ is a function only of the initial length scale (l_s) of the scalar field. Clearly, ϵ_l decays monotonically in time, the rate of decay being larger for smaller l_s and *vice-versa*. The non-monotonic behavior of ϵ_s in the DNS

data of Eswaran and Pope (1988) for large l_s (small k_s) is, then, entirely due to $\langle S(t) \rangle$. We can write

$$\frac{d \ln \epsilon_s}{dt} = p(t) + \frac{d \ln \epsilon_l}{dt} \tag{58}$$

If ϵ_s is to grow in time, we need $p(t)$ (which is always positive) to be greater in magnitude than the decay rate of $\ln \epsilon_l$. This can happen for small k_s when the decay of ϵ_l is slow enough and when $p(t)$ is near its maximum ($t = t_m$). At later times, when $p(t)$ settles down at is smaller asymptotic value, ϵ_s will decrease due to the influence of ϵ_l. For the case of large k_s, the decay rate of $\ln \epsilon_l$ is always much larger in magnitude than $p(t)$. Hence, for these values of k_s, ϵ_s decreases monotonically.

3.2 Pdf of scalar dissipation

Eswaran and Pope (1988) find that at long times, the pdf of scalar dissipation is log-normal in the presence of isotropic turbulence. As mentioned in the previous Section, the pdf of scalar dissipation in the absence of the velocity field is not log-normal. We now investigate if our present analysis of the role of the velocity field can predict log-normality of the scalar dissipation.

Let $\theta (= \frac{\partial \phi}{\partial X_i} \frac{\partial \phi}{\partial X_i})$ be the instantaneous value of the scalar dissipation. As before, we can write

$$\theta(t) = T_{ab}(t) \theta^l_{ab}(t), \tag{59}$$

where

$$\theta^l_{ab} = \frac{\partial \phi}{\partial x_a} \frac{\partial \phi}{\partial x_b} \quad \text{and} \quad T_{ab} = \frac{C_{ia}}{V} \frac{C_{ib}}{V}.$$

The matrix $\mathbf{T}$ is symmetric and positive definite. At long times, it would not be unreasonable to expect the relative orientation of the principal axes of $\mathbf{T}$ and the tensor θ^l_{ab} to reach a stationary state. Then,

$$\theta(t \to \infty) \sim |T(t)||\theta^l(t)|, \tag{60}$$

where $|T|$ and $|\theta^l|$ are the norms. This can be further simplified as

$$\theta(t \to \infty) = \frac{A^2(t)}{V^2(t)}|\theta^l(t)|, \tag{61}$$

where $A(t)$ again represents the area of a typical material surface associated with the fluid element. The physical meaning of this approximation is that at long times, the smallest length scale associated with a material element is the volume (of the fluid-element) divided by the area of a typical surface element. The scalar dissipation, being the square of the scalar gradient, should be inversely proportional to the square of the smallest length scale. So, at long times,

$$\ln(\theta) \sim \ln(|\theta^l|) + 2\ln(A) - 2\ln(V). \tag{62}$$

In incompressible turbulence, $V(t) = 1$ and, hence, $\ln(V) = 0$. During the final stages of mixing, as the fluctuations in $|\theta^l|$ die out, the only fluctuations in the scalar dissipation are due to $A(t)$. As mentioned before, in isotropic turbulence, the area of a surface element is log-normally distributed. Hence, the scalar dissipation at long times is also log-normal, and the log-normality is entirely the doing of the velocity field.

4 Mixing from non-standard initial conditions

In Section 2 it was shown that, for the case of equal-quantity, non-premixed initial fields, the HCS scalar pdf and DNS scalar pdf are quite similar at all stages of decay. It is reasonable, then, to expect that the pdf's of the heat conduction equation and full turbulence equation are similar for mixing from other initial conditions also, as long as the initial field is prescribed in a random manner. The effect of the velocity field on these non-standard mixing processes will be the same as that on the equal-quantity, non-premixed mixing. Recall that, throughout the analysis in Section 3, the only restrictions on the initial scalar field are that the field is random and isotropic. The assumption in equation (36) is valid for any scalar field that meets the above requirements.

In this Section, we study scalar fields evolving according to the heat conduction equation from non-standard initial conditions. Another important objective is to determine if the β-pdf model replicates the pdf's well for the case of non-equal, non-premixed initial fields.

4.1 Non-equal, non-premixed initial fields

In this subsection, we study the mixing of scalars from the following four initial conditions:

$$F_1(\psi,0) = .85\delta(\psi) + .15\delta(1-\psi),\ \mu = 0.15, \tag{63}$$

$$F_2(\psi,0) = .8\delta(\psi) + .2\delta(1-\psi),\ \mu = 0.20, \tag{64}$$

$$F_3(\psi,0) = .7\delta(\psi) + .3\delta(1-\psi), \mu = 0.30, \tag{65}$$

$$F_4(\psi,0) = .6\delta(\psi) + .4\delta(1-\psi), \mu = 0.40, \tag{66}$$

with $k_s = 8$.

In Figure 9, the pdf of mass fraction at various stages of decay are plotted for the case of $\mu = 0.3$. The HCS data is compared with the β-pdf model at the corresponding value of mean and variance (Girimaji 1991a). The β-pdf model appears to match the the data quite well over all stages of the mixing process.

In Figure 10, the flatness-factor (S_4) of the mass fraction is plotted against variance for initial fields of various different μ's. Figure 11 represents a similar plot for the super-skewness (S_6). With decreasing mean, the initial values of flatness-factor and super-skewness increase:

$$S_n(0) = \frac{(1-\mu)^{n-1} + \mu^{n-1}}{[\mu(1-\mu)]^{\frac{n}{2}-1}}. \tag{67}$$

For $\mu = 0.4$ and $\mu = 0.3$, S_4 and S_6 are monotonic functions of variance, going to the Gaussian values of 3 and 15, respectively, at long times. However, for smaller μ's (0.2 and 0.15), S_4 and S_6 increase with variance, overshooting the Gaussian values at the early stages and then decay slowly, asymptoting to their respective Gaussian values at long times. The smaller the mean, the more pronounced is the non-monotonic behavior. The β-pdf-model values of S_4 and S_6 are also plotted in Figures 10 and 11. The model compares quite well with HCS data for S_4 and adequately well for S_6. The model captures the non-monotonic behavior of the moments very well.

Conditional scalar dissipation. The good agreement between HCS and the β-pdf model begs the question, how does the conditional dissipations compare? In Figure 12, the fractional dissipation ($F_1(\psi)\chi(\psi)/\epsilon_s$) obtained

from HCS is compared with the model M1 (equation 28). The agreement is excellent over all stages of the mixing process.

An important issue that has been brought up in the recent works of O'Brien and Jiang (1991) and Girimaji (1992) is whether the conditional scalar dissipation for non-equal, non-premixed mixing, is symmetric about $\psi = 0.5$. The closure-mapping-based model of O'Brien and Jiang (1991) suggests that the conditional dissipation is symmetric, whereas the model of Girimaji (1992) suggests that it is not. Although Girimaji (1992) presents qualitative reasons that the latter should be the case, no direct verification has been possible due to the lack of corresponding DNS data. In Figure 13, the conditional dissipation calculated from HCS (for the case $\mu = 0.3$) is plotted at various stages of scalar decay. As mentioned in Section 2, this statistic is more error-prone than fractional dissipation. Despite the unsmooth data, the following aspects of conditional dissipation are clear. At early stages of mixing, the conditional dissipation is symmetric about $\psi = 0.5$. However, with progressing time, the conditional dissipation gets skewed, with the maximum migrating towards the mean (0.3 in this case), as suggested by the model of Girimaji (1992). The conditional-dissipation estimate in the vicinity of $\psi = 0.3$ is quite reliable because of the high probability density in that neighborhood. As in the case of $\mu = 0.5$, in this case also, we can expect ϕ_{min} and ϕ_{max} to migrate towards $\phi = \mu$ with increased mixing.

4.2 Partially-mixed initial field

The main objectives of studying partially-mixed initial fields are (i) to determine if there is any qualitative difference in the long-time behavior and

(ii) to determine the degree of deviation from the β-pdf model calculations. (The β-pdf model cannot accommodate partially-mixed initial conditions.) The choice of partially-mixed initial fields is too numerous to cover all types of such fields. We consider the following three cases of initial pdf's:

$$F_1(\psi,0) = 0.3\delta(\psi) + 0.2\delta(\psi - 0.25) + 0.2\delta(\psi - 0.75) + 0.3\delta(\psi - 1) \quad (68)$$

$$F_2(\psi,0) = 0.45\delta(\psi) + 0.21\delta(\psi - 0.75) + 0.34\delta(\psi - 1), \quad (69)$$

$$F_3(\psi,0) = 0.5\delta(\psi) + U(0.5,1), \quad (70)$$

where $U(0.5,1)$ represents the pdf of unit probability density uniform over the range (0.5, 1.). For these three cases, the means of the distributions are 0.5, 0.5, and 0.35, respectively. Again, $k_s = 8$ for all the simulations.

In Figure 14, the pdf's of case 2, $F_2(\psi,t)$, obtained from HCS are plotted at various stages of scalar decay. At early times, we have a triple-delta pdf. The delta-function at $\psi = .75$ is smeared out very rapidly at a rate disproportionate to the leveling out of the delta peaks at zero and unity. Very soon the scalar pdf appears like that of non-premixed initial fields (e.g., Figure 1). As expected, the β-pdf model does not capture the intermediate peak in the early stages, but, as this peak is smeared out, the β pdf compares quite well with the HCS data.

In Figure 15, the flatness-factors (S_4) of the three cases are plotted against the variance. The model values of S_4 for the given value of mean and variance are also plotted in Figure 15. Figure 16 represents a similar plot of super-skewness. Our observations from Figure 15 and 16 are

1. All the cases appear to tend to the Gaussian asymptotic state.

2. The β-pdf model agrees tolerably well with cases 1 and 2.

3. The agreement between case 3 and the corresponding β-pdf model is not as good. For this case, the HCS moments S_4 and S_6 decrease with variance at the very early stages and then increase to Gaussian values. However, the model values grow monotonically to Gaussian values and are always higher than HCS values.

5 Summary and conclusions

This work represents an effort to improve our understanding of passive-scalar mixing in an isotropic turbulence velocity field. The most important contribution of this study is that it presents a simple, yet quantitative picture of turbulent mixing which adequately explains all of the known and observed behavior of such a mixing process. The findings of this study should simplify the modeling of turbulent mixing. The following is a brief summary of the findings.

1. Many aspects of the scalar-pdf evolution in isotropic turbulence observed by Eswaran and Pope (1988) are the consequences of the effect of molecular diffusion on the initial random scalar field, rather than the effects of the velocity field itself.

2. The effect of the velocity field is identified, isolated, and quantified. The velocity field manifests itself on molecular mixing via the quantity $S(t)$ (equation 38) and only affects the time scale of the scalar pdf evolution. The analysis performed in Section 3 is valid for any velocity field that is isotropic and has a length scale larger than that of the scalar field. Hence, irrespective of whether the velocity field is

incompressible, compressible, or even evolving according to equations other than Navier-Stokes, we can expect the shape of the scalar pdf to evolve in the same universal manner.

3. The following model for mean scalar dissipation is provided (rewriting equation 58)

$$\frac{d\epsilon_s}{dt} \sim \epsilon_s(0.8\sqrt{\frac{\epsilon}{\nu}} + \frac{d\ln\epsilon_l}{dt}), \tag{71}$$

where ϵ is the mechanical dissipation of the turbulent field, ν is the kinematic viscosity, and the second term on the right-hand side is a function of the initial spectrum and the diffusivity of the scalar field. This expression should provide a foundation on which realistic models for mean scalar dissipation can be constructed in the future. The model for ϵ_s that is currently in use is

$$\epsilon_s = C_1\sigma_s^2\frac{\epsilon}{k}, \tag{72}$$

where C_1 is a numerical constant and k is the turbulent kinetic energy. This model is independent of the length scale or the diffusivity of the scalar field and, hence, unrealistic.

4. An explanation for the observed log-normality of the scalar dissipation is provided. A qualitative explanation for the log-normality was given previously by Hill and Bowhill (1978). Despite that, the present model represents an important contribution towards understanding turbulent mixing for, not only is it quantitative (relating the scalar dissipation to known turbulence parameters via material element deformation statistics), but it is also a part of a larger model which incorporates all the observed properties of turbulent scalar mixing.

5. Analytical arguments and numerical evidence are presented questioning the asymptotic correctness of the mapping-closure-based conditional scalar dissipation model of O'Brien and Jiang (1991), even for the case of molecular mixing (for which it is supposed to be most appropriate).

6. It is demonstrated that even for the case of non-equal, non-premixed initial fields, the β-pdf model performs quite well (Figure 9 - 11). Further, the β-pdf-based conditional dissipation model (Girimaji 1992) agrees quite well with the HCS data (Figure 12). So, the conclusion is that the β pdf is a good model for all non-premixed initial conditions.

The methodology developed in this paper can be used to address several issues regarding chemical reactions in turbulent flows. Since chemical reaction is a process that is local in space, several of the processes that need to be modeled in turbulent combustion are also local in space and, hence, can be investigated in the absence of the velocity field. A study of a random scalar field of several species undergoing molecular diffusion and chemical reaction will be useful in assessing the effect of reaction on concentration fluctuations, the importance of temperature-concentration correlations, etc.

Acknowledgements. I would like thank Dr. J. P. Drummond for his encouragement and support. This work was supported by the Theoretical Flow Physics Branch, Fluid Mechanics Division, NASA Langley Research Center, Hampton, VA 23665, under contract No. NAS1 - 18599.

References

[1] Chen, H., Chen, S., and Kraichnan, R. H. (1989). *Probability distribution of a stochastically advected scalar field.* Physical Review Letters, **63** (24), pp 2657 - 2660.

[2] Eswaran, V., and Pope, S. B. (1988). *Direct Numerical Simulations of the turbulent mixing of a passive scalar.* Physics of Fluids, **31** (3), pp 506 - 520.

[3] Gao, F. (1991). *An analytical solution for the scalar probability density function in homogeneous turbulence.* Phys. Fluids A, **3** (4), 511 - 513.

[4] Girimaji, S. S., and Pope, S. B. (1990). *Material element deformation in isotropic turbulence* J. Fluid Mech. **220**, pp 427 - 458.

[5] Girimaji, S. S. (1991a). *Assumed β-pdf model for turbulent mixing: validation and extension to multiple scalar mixing.* Combust. Sci. and Tech. **78**, 4 - 6, pp 169.

[6] Girimaji, S. S. (1991b). *A simple recipe for modeling reaction-rates in flows with turbulent combustion.* AIAA-91-1792. AIAA 22nd Fluid Dynamics, Plasma Dynamics and Lasers Conference, June 24-26, 1991, Honolulu, Hawaii.

[7] Girimaji, S. S. (1992). *On the modeling of scalar diffusion in isotropic turbulence.* To appear in Phys. Fluids. A.

[8] Givi, P. (1989). *Model-free simulations of turbulent reactive flows.* Progress in Energy and Combustion Science, **15** (1), pp 1 - 107.

[9] Givi, P., Madnia, C. K., Steinberger, C. J., and Tsai, A. (1991) *Large eddy simulations and direct numerical simulations of high speed turbulent reacting flows.* State University of New York report, Department of Mechanical Engineering, SUNY, Buffalo, NY 14280.

[10] Hill, R. J., and Bowhill, S. A. (1978). *Lognormality of gradients of advected scalars.* Physics of Fluids, **21** (6), pp 883 - 886.

[11] Monin, A. S., and Yaglom, A. M. (1981). *Statistical fluid mechanics,* Vol. 2 (ed. J. L. Lumley), MIT Press.

[12] O'Brien, E. E., and Jiang, T-L (1991). *The conditional dissiption rate of an initially binary scalar.* Physics of Fluids, **3**, 3121 - 3123.

[13] Pope, S. B. (1985). *Pdf methods for turbulent reactive flows.* Progress in Energy and Combustion Science, **11**, pp 119 - 192.

[14] Pope, S. B. (1991). *Mapping closures for turbulent mixing and reaction.* Theoretical and Computational Fluid Dynamics, **2**, 255 - 270.

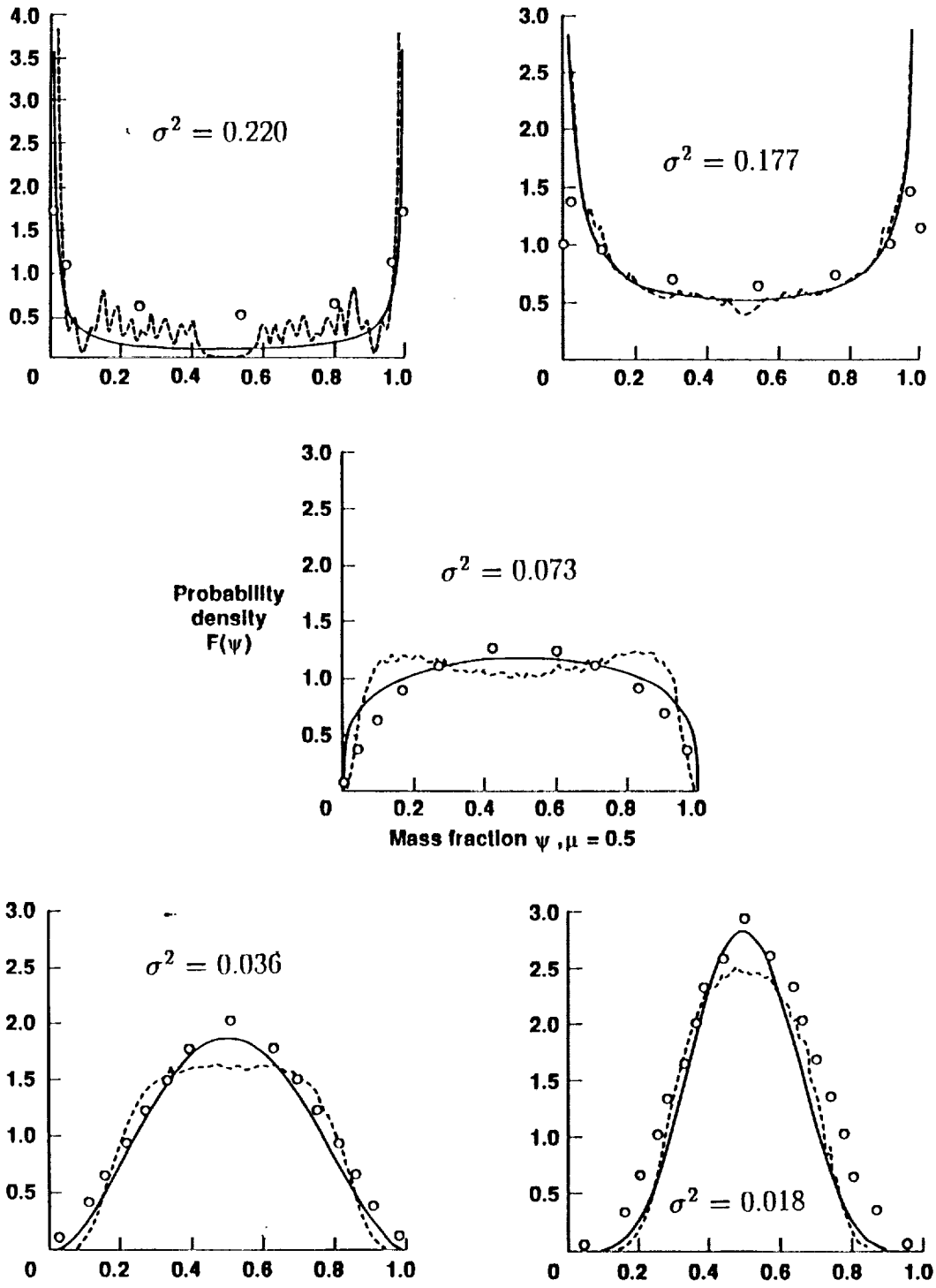

Figure 1: Evolution of scalar pdf, $F(\psi)$, for the case of $\mu = 0.5$. Circles represent DNS data, dashed line represents HCS data, and solid line represents β-pdf model calculations.

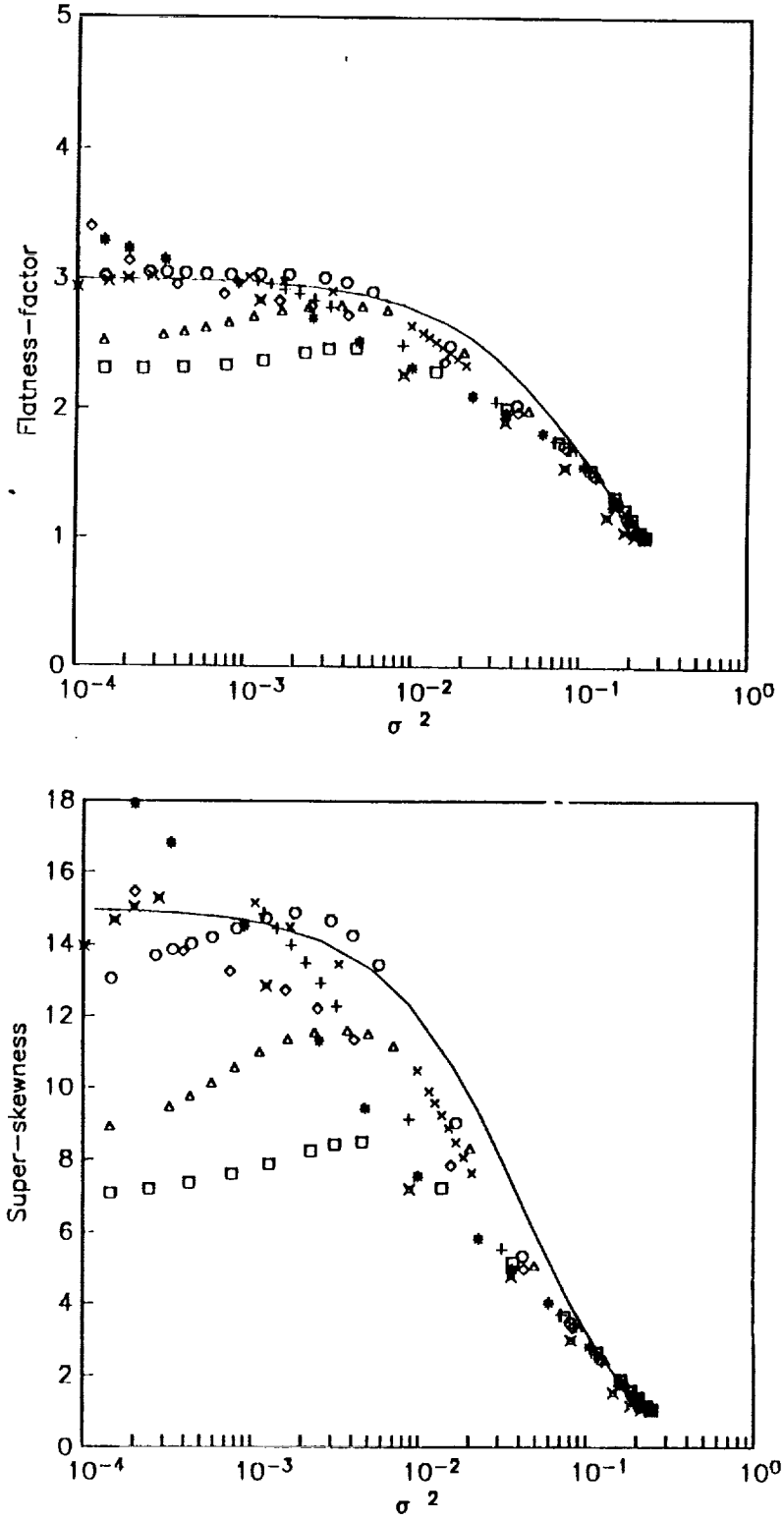

Figure 2: (a) HCS scalar flatness-factor vs. scalar variance and (b) scalar super-skewness vs. scalar variance, for the case of $\mu = 0.5$. ($\square$ $k_s = 1$; $\triangle$ $k_s = 2$; $\bigcirc$ $k_s = 4$; $\diamond$ $k_s = 6$; $+$ $k_s = 8$; $*$ $k_s = 10$; $\times$ $k_s = 12$; $\blacksquare$ $k_s = 16$; solid-line β-pdf model.)

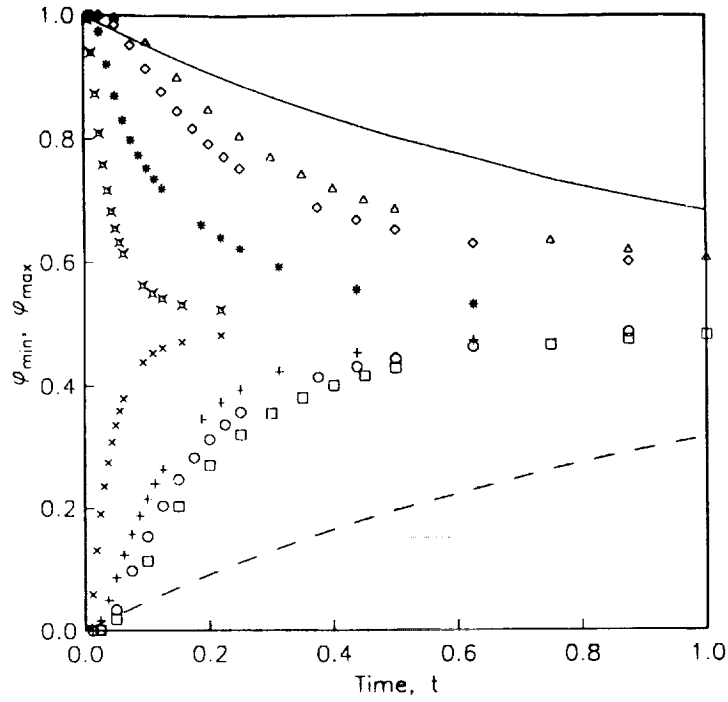

Figure 3: Temporal evolution of ϕ_{min} and ϕ_{max} for various initial length scales. ($\square$ - $\phi_{min}(k_s = 1)$; $\triangle$ - $\phi_{max}(k_s = 2)$; $\bigcirc$ - $\phi_{min}(k_s = 2)$; $\diamond$ - $\phi_{max}(k_s = 2)$; $+$ - $\phi_{min}(k_s = 4)$; $*$ - $\phi_{max}(k_s = 4)$; $\times$ - $\phi_{min}(k_s = 8)$; $\blacksquare$ - $\phi_{max}(k_s = 8)$; solid line correspond to $\phi_{max} = \frac{1}{2} + \frac{1}{2}exp[-t]$ and and the dashed line to $\phi_{min} = \frac{1}{2} - \frac{1}{2}exp[-t]$.)

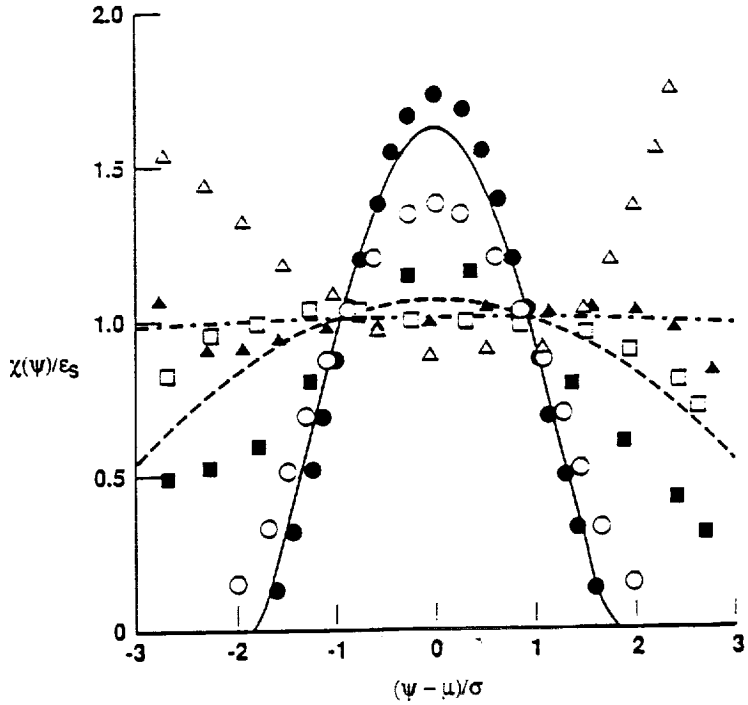

Figure 4: Conditional scalar dissipation ratio vs. Normalized Mass Fraction for the case of $\mu = 0.5$. Comparison of DNS data, HCS data and model M1 (Girimaji 1991b). ($\sigma = 0.27$: — DNS, $\bigcirc$ model, $\bullet$ HCS; $\sigma = 0.10$: - - - DNS, $\square$ model, $\blacksquare$ HCS; $\sigma = 0.02$: - · - DNS, $\triangle$ model, $\blacktriangle$ HCS.)

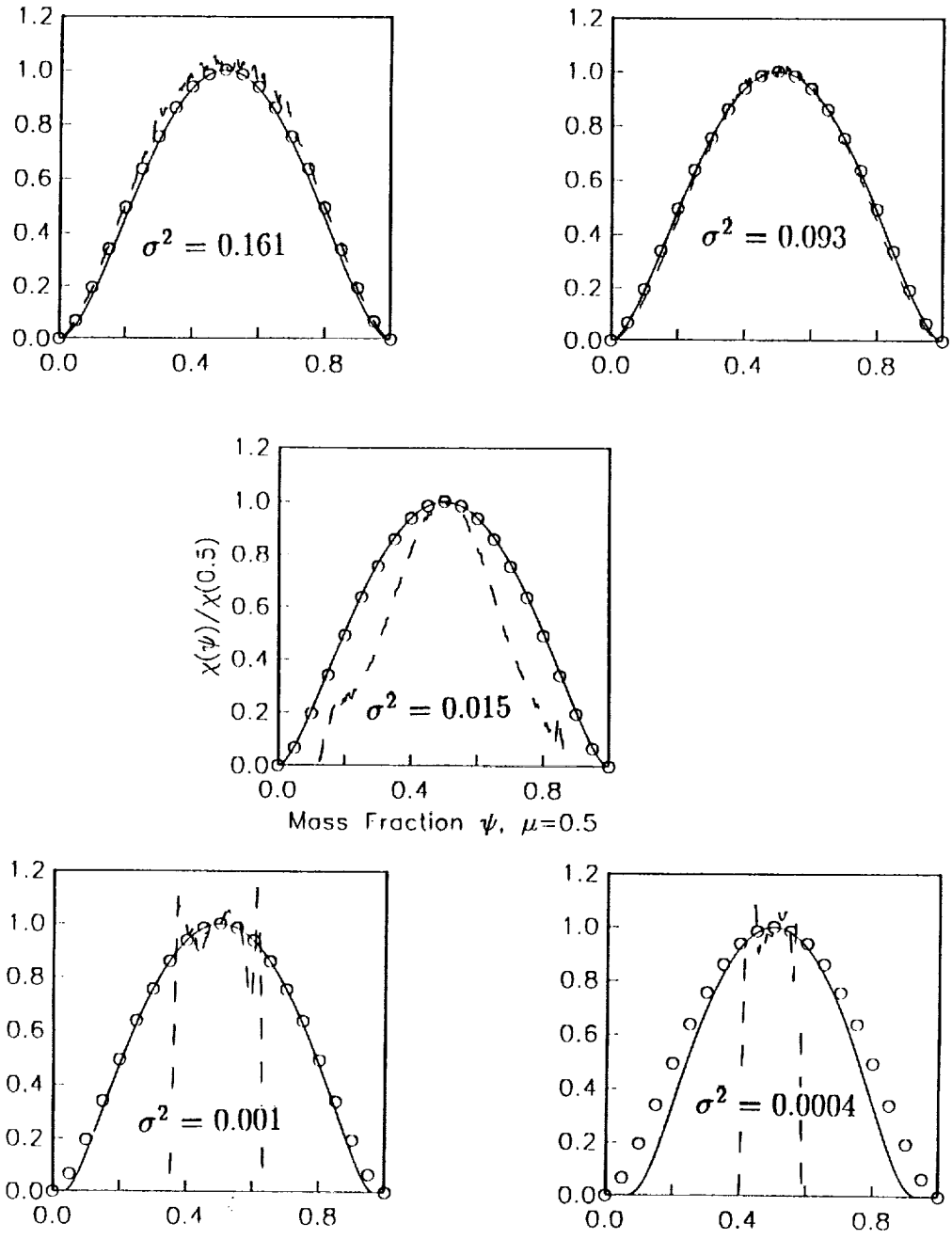

Figure 5: Evolution of normalized scalar dissipation, $\chi(\psi)/\chi(0.5)$, for the case of $\mu = 0.5$. Circles represent model M2 (Gao 1991), dashed line represents IICS data, and solid line represents model M1.

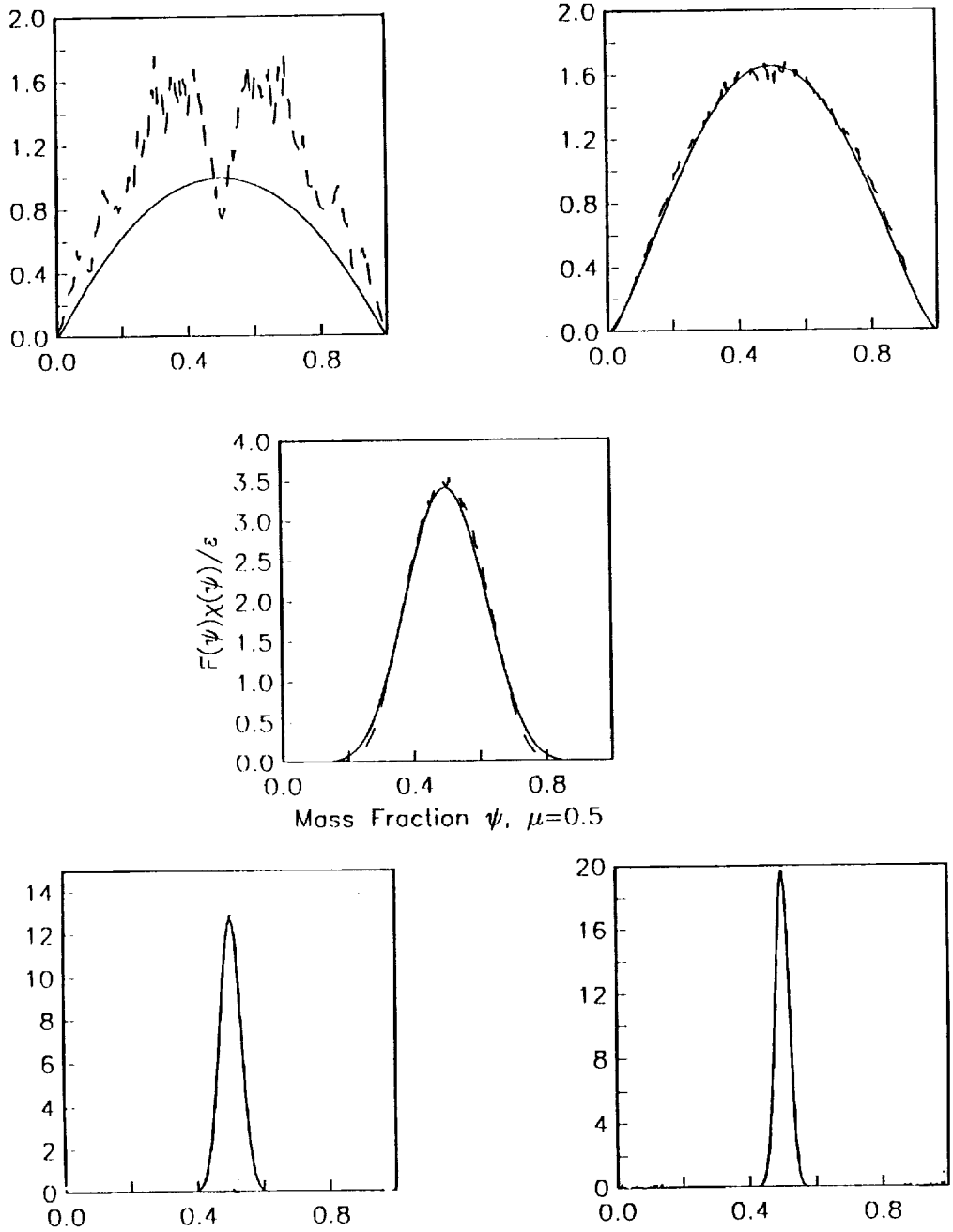

Figure 6: Evolution of fractional scalar dissipation, $F(\psi)\chi(\psi)/\epsilon_s$, for the case of $\mu = 0.5$. Dashed line represents HCS data and solid line represents model M1 (Girimaji 1991b).

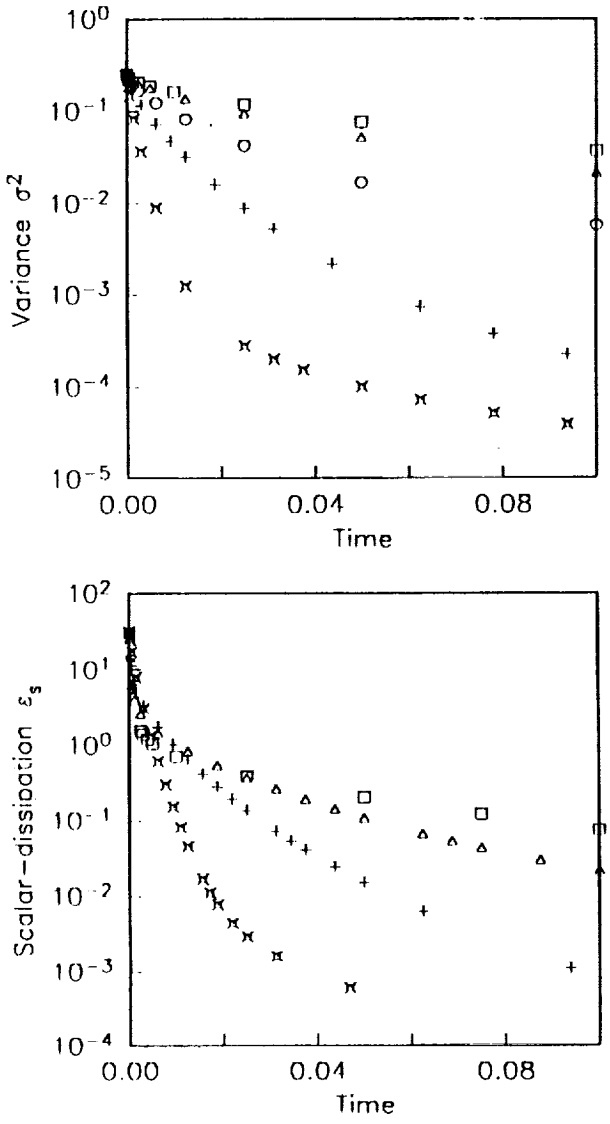

Figure 7: Evolution of HCS scalar variance and mean scalar dissipation for the case of $\mu = 0.5$. (Symbols same as in Figure 2.)

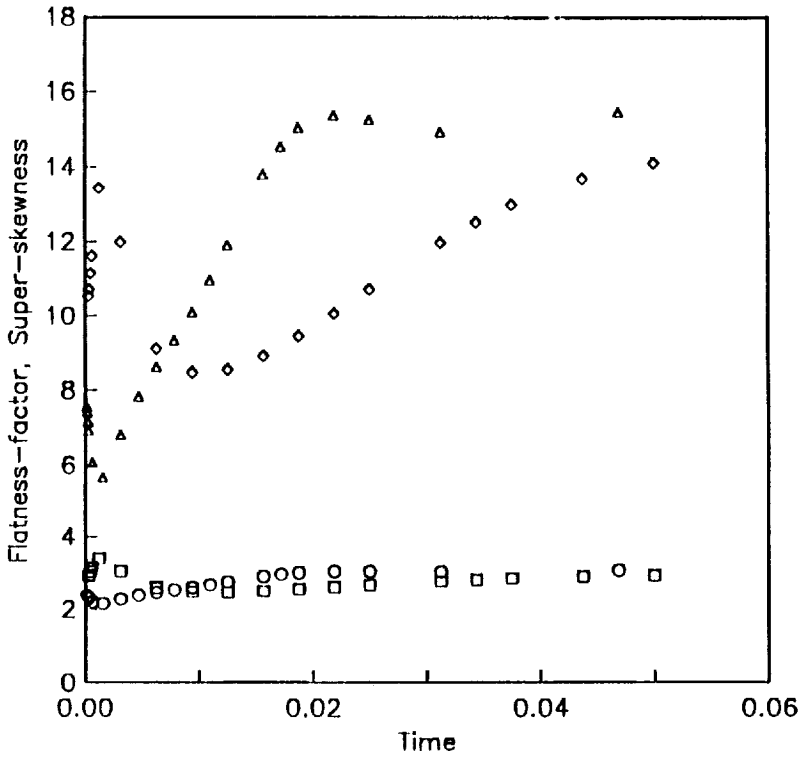

Figure 8: Evolution of HCS flatness-factor and super-skewness of scalar-gradient $\partial\phi/\partial x_1$ ($\mu = 0.5$). (Flatness factor: ○ $k_s = 16$; □ $k_s = 8$. Superskewness: △ $k_s = 16$; ◇ $k_s = 8$.)

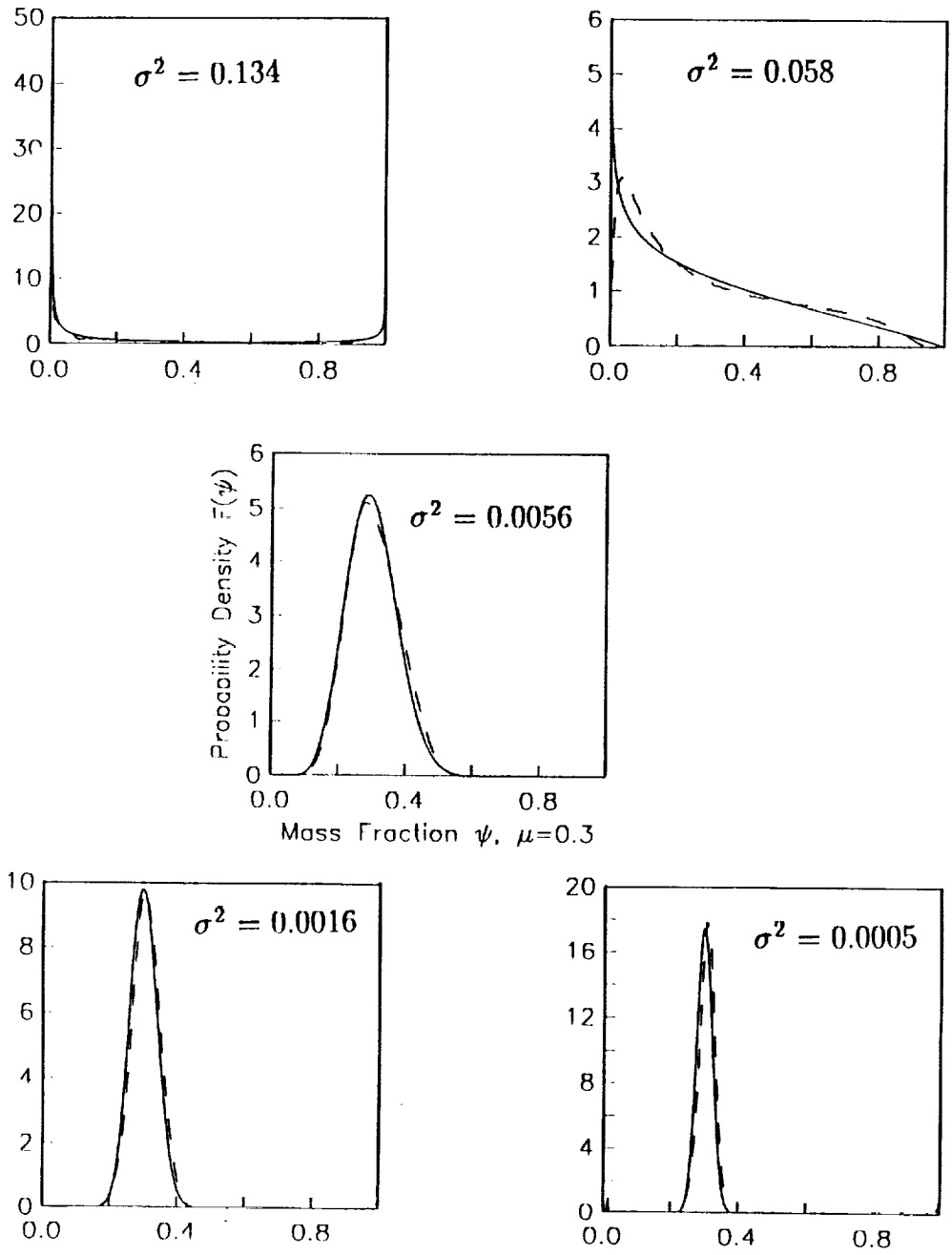

Figure 9: Evolution of scalar pdf, $F(\psi)$, for the case of $\mu = 0.3$. Dashed line represents HCS data, and solid line represents β-pdf model calculations.

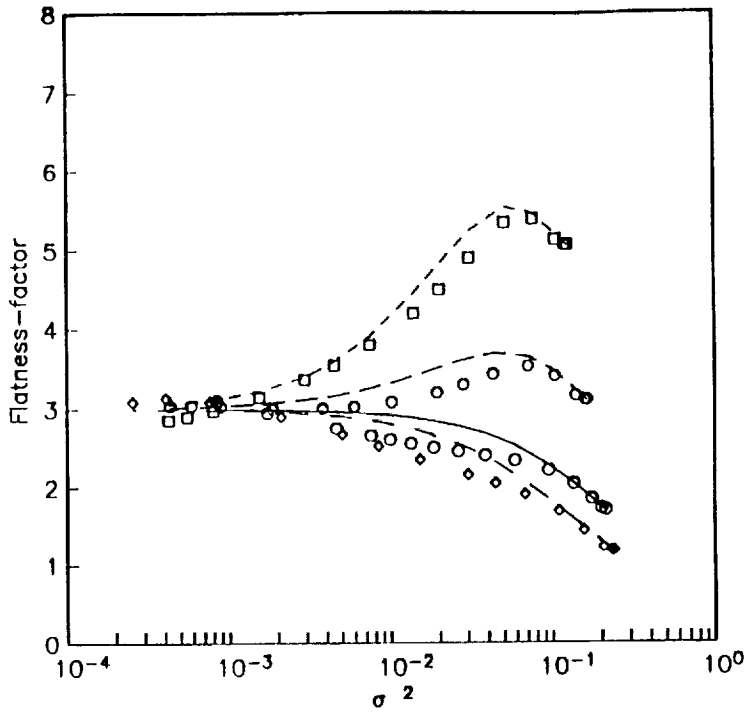

Figure 10: Scalar flatness-factor vs. scalar variance for non-equal non-premixed initial conditions. ($\mu = 0.15$: □, HCS; - - - - β-pdf model. $\mu = 0.20$: ⬡(*hexagon*), HCS; — — β-pdf model. $\mu = 0.30$: ○, HCS; — β-pdf model. $\mu = 0.40$: ◇, HCS; - - - β-pdf model.)

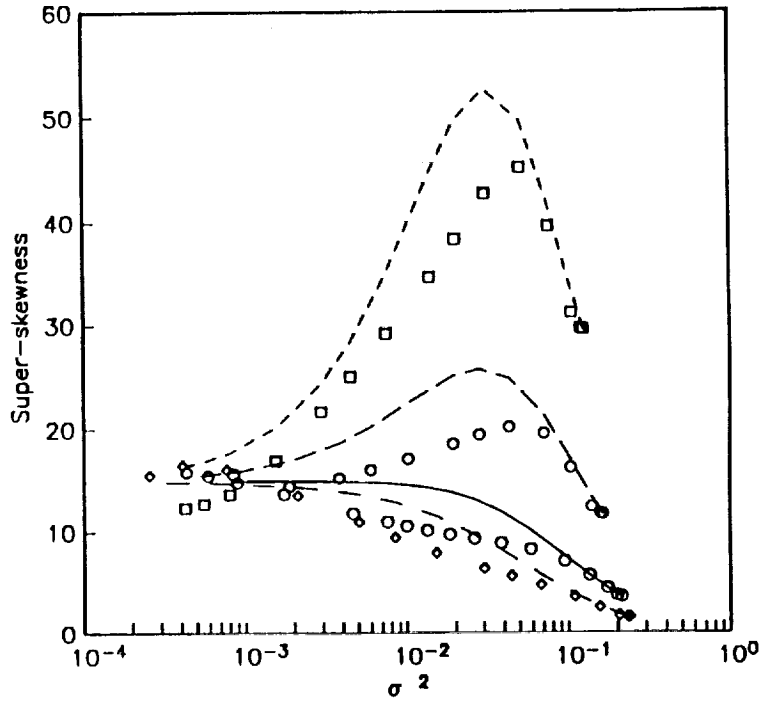

Figure 11: Scalar super-skewness vs. scalar variance for non-equal non-premixed initial conditions. (Symbols same as Figure 10.)

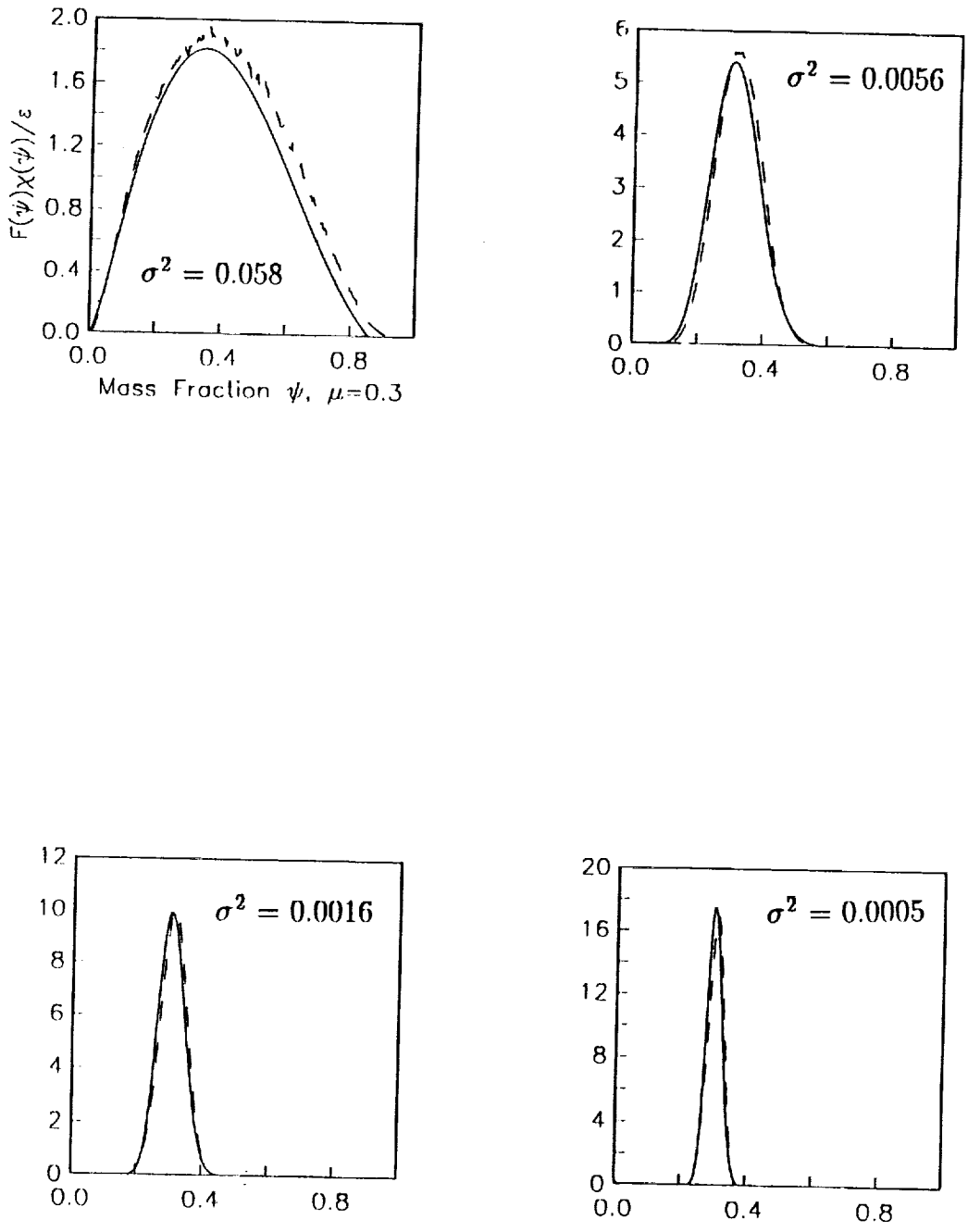

Figure 12: Evolution of fractional scalar dissipation, $F(\psi)\chi(\psi)/\epsilon_s$, for the case of $\mu = 0.3$. Dashed line represents HCS data and solid line represents β-pdf model calculations.

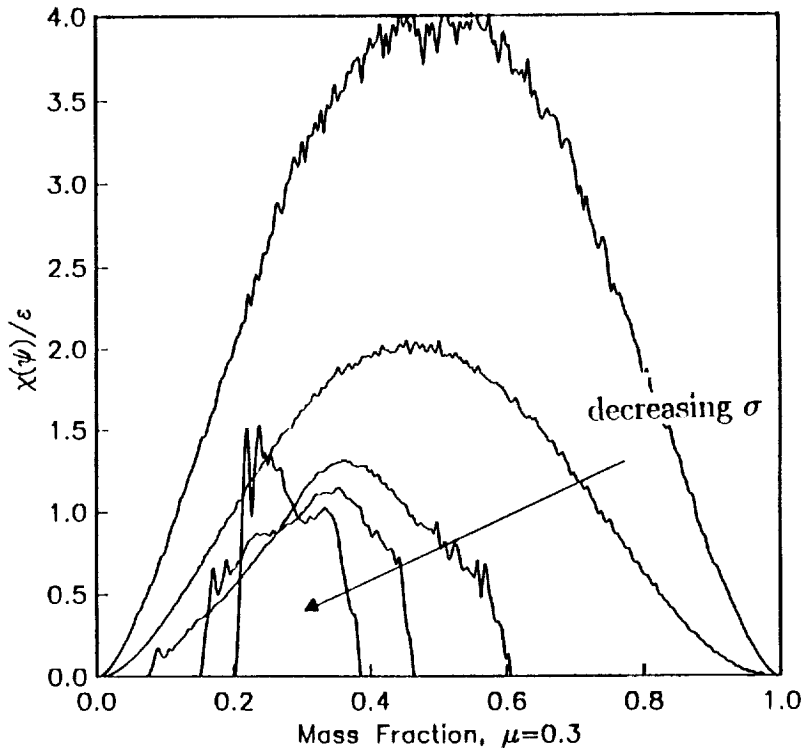

Figure 13: Evolution of conditional scalar dissipation, $\chi(\psi)/\epsilon_s$, for the case of $\mu = 0.3$. HCS data.

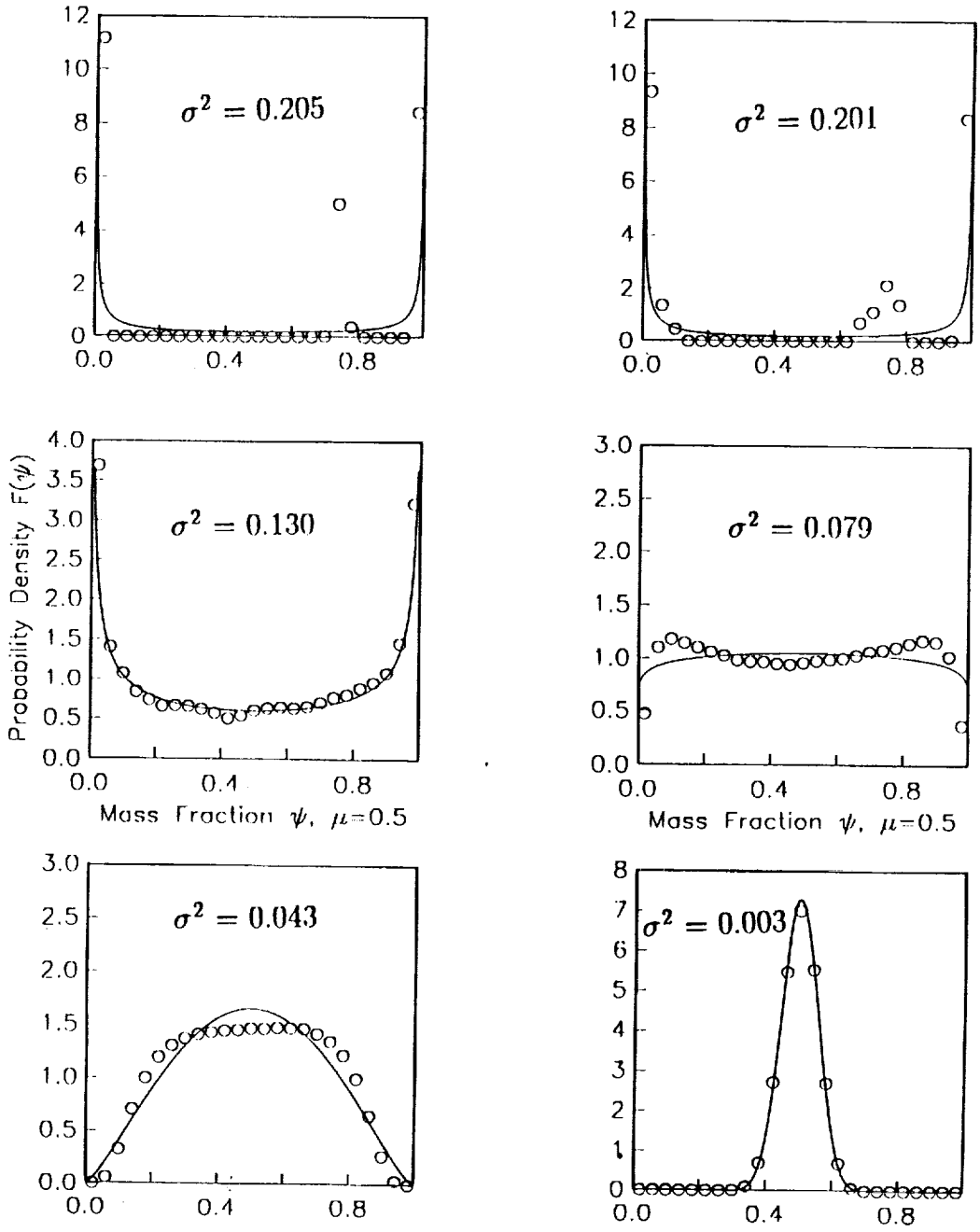

Figure 14: Evolution of scalar pdf, $F(\psi)$, for partially-mixed initial field, Case 2 of subsection 4.2. Circles represent HCS data and solid line represents β-pdf model calculations.

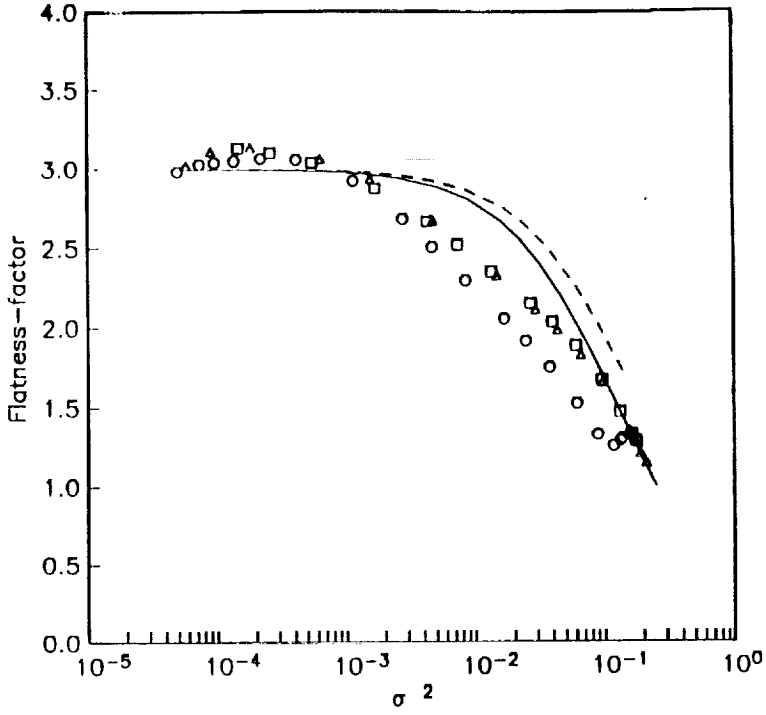

Figure 15: Scalar flatness-factor vs. scalar variance for partially-mixed initial conditions. (□ and △ represent HCS data of Cases 1 and 2 of Section 4.2. The solid line represents the β-pdf model calculations corresponding to cases 1 and 2. ○ represents HCS data of Case 3, and the dashed line the corresponding model calculations.)

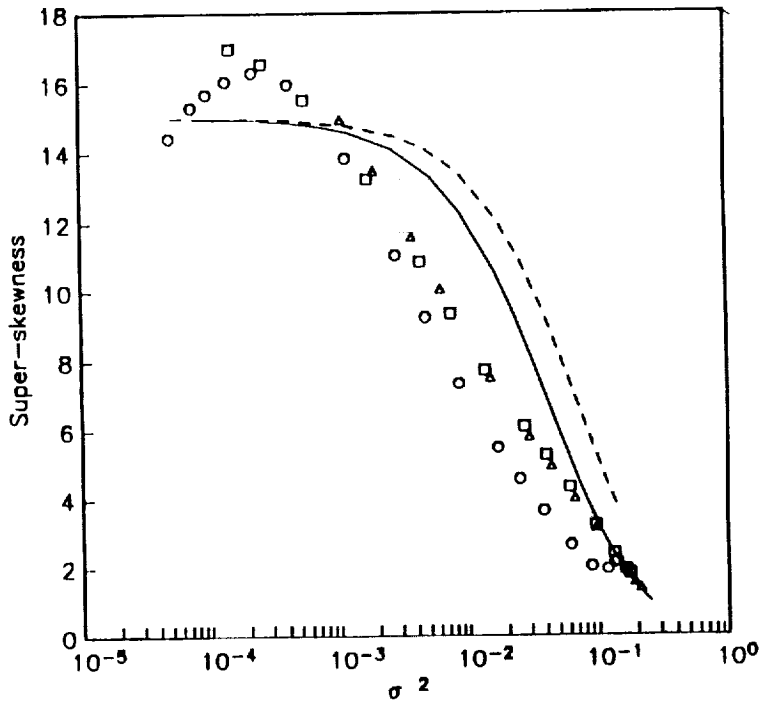

Figure 16: Scalar super-skewness vs. scalar variance for partially-mixed initial conditions. (Symbols same as Figure 15.)

REPORT DOCUMENTATION PAGE

Form Approved
OMB No. 0704-0188

1. AGENCY USE ONLY (*Leave blank*)	2. REPORT DATE	3. REPORT TYPE AND DATES COVERED
	July 1992	Contractor Report

4. TITLE AND SUBTITLE
Towards Understanding Turbulent Scalar Mixing

5. FUNDING NUMBERS
C NAS1-18599
WU 505-62-40-06

6. AUTHOR(S)
Sharath S. Girimaji

7. PERFORMING ORGANIZATION NAME(S) AND ADDRESS(ES)
Analytical Services and Materials, Inc.
107 Research Drive
Hampton, VA 23666

8. PERFORMING ORGANIZATION REPORT NUMBER

9. SPONSORING / MONITORING AGENCY NAME(S) AND ADDRESS(ES)
National Aeronautics and Space Administration
Langley Research Center
Hampton, VA 23665-5225

10. SPONSORING / MONITORING AGENCY REPORT NUMBER
NASA CR-4446

11. SUPPLEMENTARY NOTES
Technical Monitor: J. Philip Drummond

12a. DISTRIBUTION / AVAILABILITY STATEMENT
Unclassified-Unlimited

Subject Category 34

12b. DISTRIBUTION CODE

13. ABSTRACT (*Maximum 200 words*)

In an effort towards understanding turbulent scalar mixing, we study the effect of molecular mixing, first in isolation and then accounting for the effects of the velocity field. The chief motivation for this approach stems from the strong resemblance of the scalar probability density function (pdf) obtained from the scalar field evolving from the heat conduction equation and that evolving in a turbulent velocity field. However, the evolution of the scalar dissipation is different for the two cases. We attempt to account for these differences, which are due to the velocity field, using a Lagrangian frame analysis. After establishing the usefulness of this approach, we use the heat-conduction simulations (HCS), in lieu of the more expensive direct numerical simulations (DNS), to study many of the less understood aspects of turbulent mixing. Comparison between the HCS data and available models are made whenever possible. It is established that the Beta pdf characterizes, quite well, the evolution of the scalar pdf during mixing from all types of non-premixed initial conditions.

14. SUBJECT TERMS	15. NUMBER OF PAGES
turbulent-mixing models stochastic mixing	52
	16. PRICE CODE A04

17. SECURITY CLASSIFICATION OF REPORT	18. SECURITY CLASSIFICATION OF THIS PAGE	19. SECURITY CLASSIFICATION OF ABSTRACT	20. LIMITATION OF ABSTRACT
Unclassified	Unclassified		Unlimited

NSN 7540-01-280-5500

Standard Form 298 (Rev. 2-89)
Prescribed by ANSI Std. Z39-18
298-102

NASA-Langley, 1992